5.1 Preformulation studies

5.1.1 Physical observation

The color, odour, and physical appearance of the drug were physically examined and identified.

5.1.2 FTIR interpretation

The FTIR spectrum of DSB (sample drug) had shown identical peaks as reported in references sample of DSB (Figure 5.1). The FTIR spectrum has shown absorption bands as mentioned in Table 5.1.

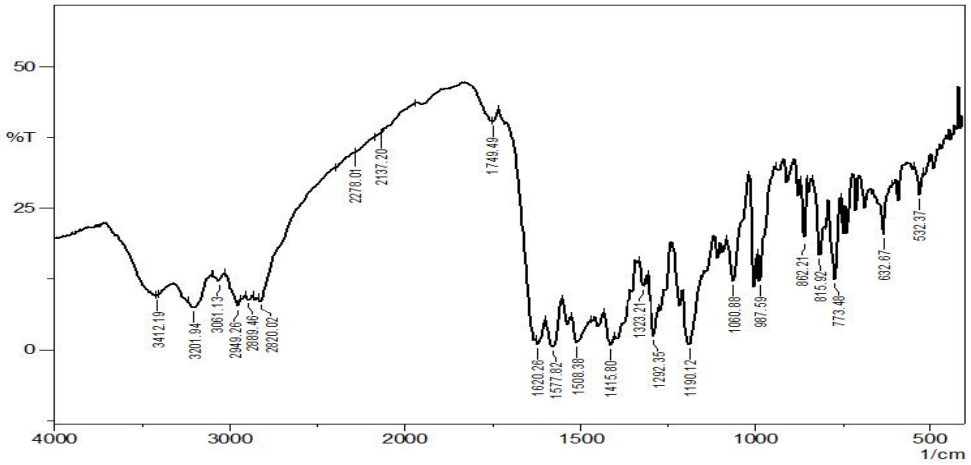

Figure 5.1 FTIR spectrum of dasatinib

Table 5.1 FTIR spectra obtained in the spectral region of 4000 to 500 cm^{-1}

Group	Dasatinib (cm^{-1})
N-H stretching	3412.19
O-H stretching	3201.94
-C-H aromatic ring	3061.13
C-H stretching	2949.26
C═O stretching	1620.26
-C-H, CH═CH	1577.82
C-Cl	773.48

5.1.3 Analytical method development for DSB by UV-Visible spectroscopy

UV-Visible spectrophotometric analytical method development was done for quantitative estimation of DSB. A standard DSB stock solution (1000 µg/ml) was freshly prepared in pH 7.4 PBS and from the standard stock solution, set of serial dilutions were made to get concentration range of 30-100 µg/ml and the resultant drug solutions were scanned for spectrum under 260 to 500 nm. The absorption maxima of the DSB solution was obtained at 325 nm as illustrated in Figure 5.2. Thus, the procured drug sample of DSB showed sharp and clear absorption maxima and complies with the reference spectrum. To plot the calibration curve of DSB, UV-Visible spectrophotometer was used in the concentration range of 30-100 µg/mL at 325 nm. Standard calibration plot of DSB was found to be linear with R^2 value 0.999, showed a proportional increase in the absorbance with increase in concentration (Figure 5.3).

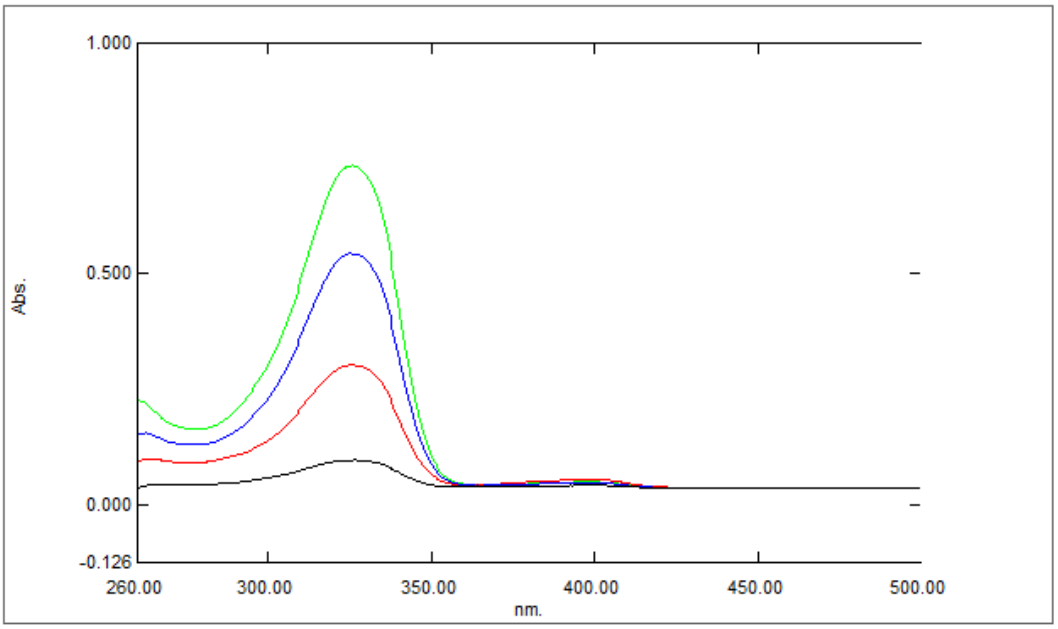

Figure 5.2 UV spectrum of Dasatinib

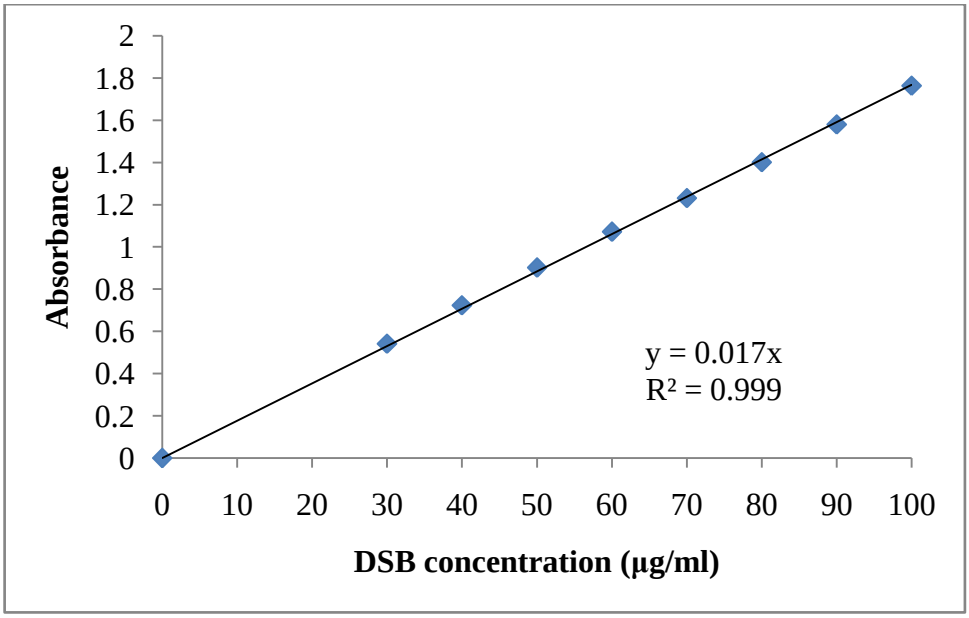

Figure 5.3 Standard calibration curve of DSB in pH 7.4 PBS at 325 nm

5.1.4 Analytical method development for biological samples (rat plasma) using HPLC and its validation

Validation of the analytical method is a process by which it is established that the performance characteristics of the analytical method meet the requirements for the proposed analytical applications. It must exhibit that the analytical method is capable to precisely and accurately predict the unknown samples concentrations. The calibration curves have thus been validated for the assay of DSB by HPLC method. C_{18} reverse phase column and a mobile phase consisting of pH 7.4 PBS:ACN was found to be appropriate for the quantitative estimation of the DSB. The HPLC analytical method was validated according to ICH guidelines and was found to be adequately sensitive and rugged for the analysis of samples. Suitability parameters such as selectivity, resolution, retention factor, and peak asymmetry were examined to determine the adequate repeatability and resolution of the proposed method. The optimal assay conditions were found by using mobile phase consisted of pH 7.4 PBS:ACN (70:30 v/v), the flow rate 1 ml/min and the column temperature of 25°C. In order to isolate the DSB from the

plasma sample deproteinization process was performed by choosing ACN as the protein precipitant as it resulted in high extraction recovery, good signal intensities, and comparatively clean chromatograms of DSB without any interfering endogenous peaks. The chromatogram of DSB in rat plasma sample spiked with a known amount of DSB is illustrated in Figure 5.4.

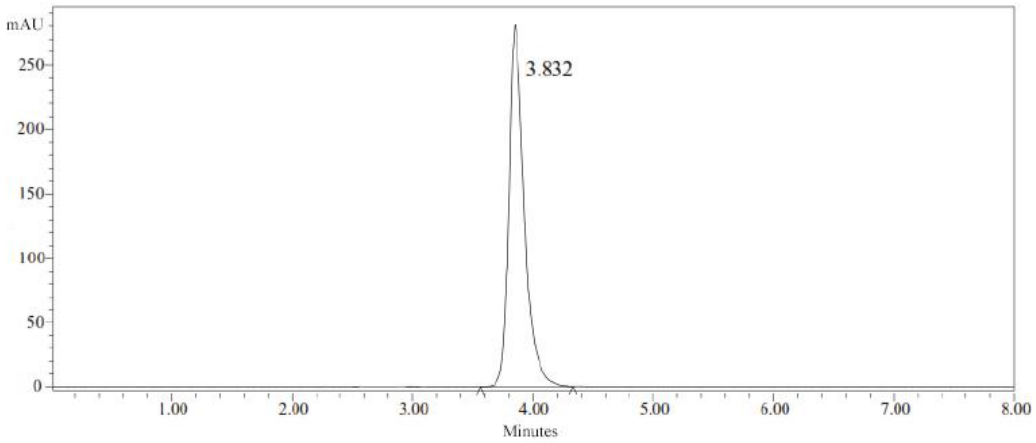

Figure 5.4 HPLC chromatogram of dasatinib spiked with rat plasma

The chromatogram was observed without any interfering peaks in the rat plasma sample. A good linear relationship was established between peak area ratios of DSB to plasma concentrations over a range of 100-2000 ng/ml (Figure 5.5). The calibration curve was found to be linear, and the correlation coefficient (r2) value generated during the validation was 0.999 (y = 172.8x - 4376), with negligible scatter of experimental points. The standard deviation of the intercept was found to be 531.8. The recovery of the DSB from the concentrations of 100-2000 ng/ml was averaged as 92.67% (Table 5.2).

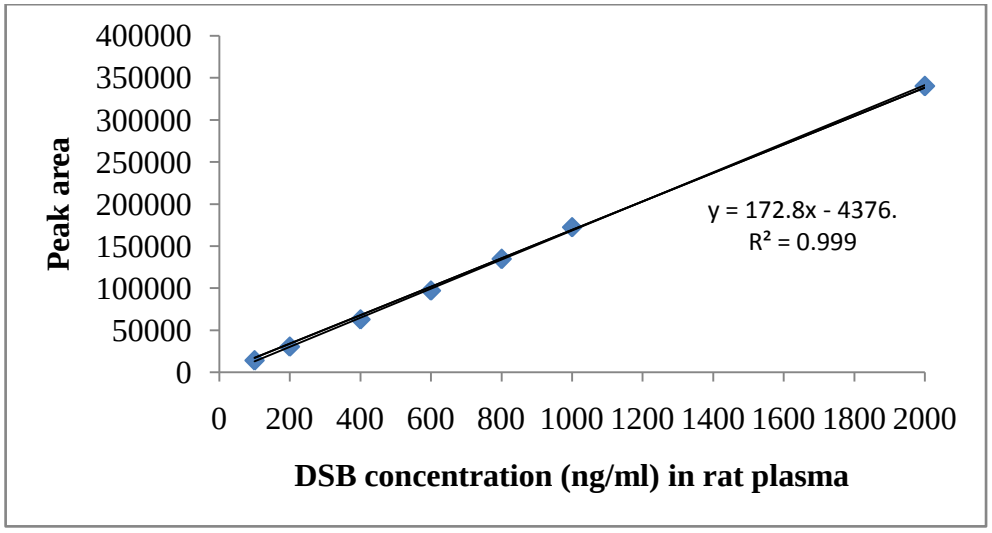

Figure 5.5 Calibration curve of dasatinib by HPLC in rat plasma

Table 5.2 Recovery of dasatinib from the rat plasma sample (n = 6)

DSB Concentration (ng/ml)	Peak area (mobile phase)	Peak area (plasma)	% Recovery
100	15149.1	13816.8	91.20
200	34663.4	30455.3	87.86
400	66376.1	62619.2	94.34
600	107768.3	96948.4	89.94
800	151706.7	134442.5	88.62
1000	176055.6	172358.4	97.90
2000	344301.9	340204.7	98.81

The precision of the analytical method was studied to find out intra-day and inter-day variation in the calibration curve of DSB. It was determined by replicate analysis of seven spiked samples with seven different concentration of DSB (100-2000 ng/ml) within one day or seven consecutive days. It was followed by the generation of calibration curves and calculation of percentage relative standard deviation (% RSD) for all the cases. The intra-day variabilities and the corresponding inter-day variabilities of standard plasma calibration curve of DSB obtained by HPLC are shown in Table 5.3

and Table 5.4, respectively. The intra-day and inter-day values of standard plasma calibration curve of DSB indicated that the optimized method is reproducible.

The accuracy of the optimized method in determining the spiked rat plasma's DSB concentrations for intra-day and inter-day are shown in Tables 5.3 and 5.4, respectively. The accuracy was represented as % bias, the values were within the range of ± 15 % and % RSD values were well below 15% over the calibration range. LOD and LOQ are two important parameters that are prerequisite for assay validation according to ICH Q2A guidelines. Under a stated experimental condition, LOD is the least possible concentration of an analyte in a sample that can be detected, but not necessarily quantitated, and LOQ is the least possible concentration of analyte in a sample that can be determined with acceptable accuracy and precision. Both were calculated based on the standard deviation of the y-intercept of the calibration curve (SD) and mean of the slope of the calibration curve (m). LOD and LOQ values of the optimized method were found to be 10.15 ng/ml and 30.77 ng/ml, respectively.

Table 5.3 Intra-day reproducibility of dasatinib standard plasma calibration curve obtained by HPLC

Intra-day	DSB concentration (ng/ml) in rat plasma						
	100	**200**	**400**	**600**	**800**	**1000**	**2000**
Mean	103.04	205.94	396.96	591.99	813.33	1017.03	2020.81
SD	±0.81	±2.40	±3.78	±3.65	±3.66	±5.17	±6.02
RSD (%)	0.784	1.163	0.953	0.616	0.450	0.508	0.298
% bias	3.040	2.97	-0.760	-1.335	1.666	1.703	1.040

Table 5.4 Inter-day reproducibility of dasatinib standard plasma calibration curve obtained by HPLC

Inter-day	DSB concentration (ng/ml) in rat plasma						
	100	**200**	**400**	**600**	**800**	**1000**	**2000**
Mean	96.88	193.74	409.28	593.52	809.90	983.50	2022.77
SD	±1.13	±3.52	±5.04	±4.95	±5.46	±18.62	±11.88
RSD (%)	1.164	1.816	1.232	0.839	0.674	1.894	0.587
% bias	-3.120	-3.130	2.320	-1.080	1.237	-1.650	1.139

The analytical method developed using HPLC was found to be sensitive enough for the quantitative determination of DSB in the biological sample (rat plasma) obtained during preclinical studies. As the optimized analytical method requires a small amount of plasma, it was found to be highly suitable for pharmacokinetic studies in small laboratory animals. The simplicity, rapidity, efficacy and short retention time of DSB made the optimized analytical method suitable for the analysis of relatively more number of plasma samples in a very short period of time providing a rapid and economical method for therapeutic monitoring in clinical laboratories.

5.2 Preparation of DSB loaded PVP stabilized chitosan capped GNPs (DSB-PVP-Ch-GNPs)

The synthesized Ch-GNPs were visually observed for the appearance of any color change in the dispersion. A clear deep ruby red color was formed within 1 hour, as a result of bioreduction by chitosan which indicated the green synthesis of Ch-GNPs and the dispersion was examined by UV-Visible spectrophotometry. The dispersion was scanned in the range of 300-800 nm wavelength. In the UV–Vis absorption spectrum, a peak maximum at 525 nm was recorded, which is attributed to the SPR band of GNPs. After the successful synthesis of Ch-GNPs, subsequent stabilization and loading of DSB were done.

5.2.1 Optimization process variables by PBD

By employing PBD, a total of 12 experimental runs were generated from eight factors, three responses, and two levels. The preliminary screening experiments with each factor (A = polymer concentration; B = stirring speed; C = stirring time; D = sonication time; E = sonication frequency; F = temperature; G = centrifugation time; H = centrifugation speed) at high and low levels and the responses (Y_1 = particle size; Y_2 = zeta potential; Y_3 = % entrapment efficiency) were evaluated and summarized in Table 5.5. The statistical evaluation was conducted by applying ANOVA, and then Pareto charts were generated in order to screen out the significant factors influencing the responses (Figure 5.6).

Table 5.5 Plackett-Burman screening design of experiment and their results

Run	A	B	C	D	E	F	G	H	Y_1*	Y_2*	Y_3*
1	-	+	-	-	-	+	+	+	36.48±0.62	-19.03±0.09	63.49±0.31
2	+	+	+	-	+	+	-	+	36.90±0.43	-15.08±0.06	52.94±0.18
3	-	+	+	-	+	-	-	-	23.42±0.19	-18.49±0.10	38.79±0.82
4	+	+	-	+	-	-	-	+	33.69±0.34	-13.51±0.04	73.94±0.13
5	-	-	-	+	+	+	-	+	30.48±0.39	-15.59±0.03	38.94±0.24
6	+	-	+	+	-	+	-	-	28.64±0.22	-14.62±0.08	74.91±0.39
7	-	-	+	+	+	-	+	+	20.24±0.46	-16.72±0.04	57.32±0.44
8	-	-	-	-	-	-	-	-	41.31±0.69	-14.13±0.03	49.72±0.36
9	-	+	+	+	-	+	+	-	18.68±0.27	-19.46±0.05	67.97±0.74
10	+	-	+	-	-	-	+	+	37.92±0.39	-12.24±0.09	63.49±0.31
11	+	+	-	+	+	-	+	-	31.12±0.62	-13.25±0.08	69.92±0.44
12	+	-	-	-	+	+	+	-	38.68±0.24	-13.87±0.10	57.94±0.63

(Note: + high level, - low level; * Mean ± SD, n = 3)

[A - polymer concentration; B - stirring speed; C - stirring time; D - sonication time; E - sonication frequency; F - temperature; G - centrifugation time; H - centrifugation speed); Y_1 - particle size; Y_2 - zeta potential; Y_3 - % entrapment efficiency].

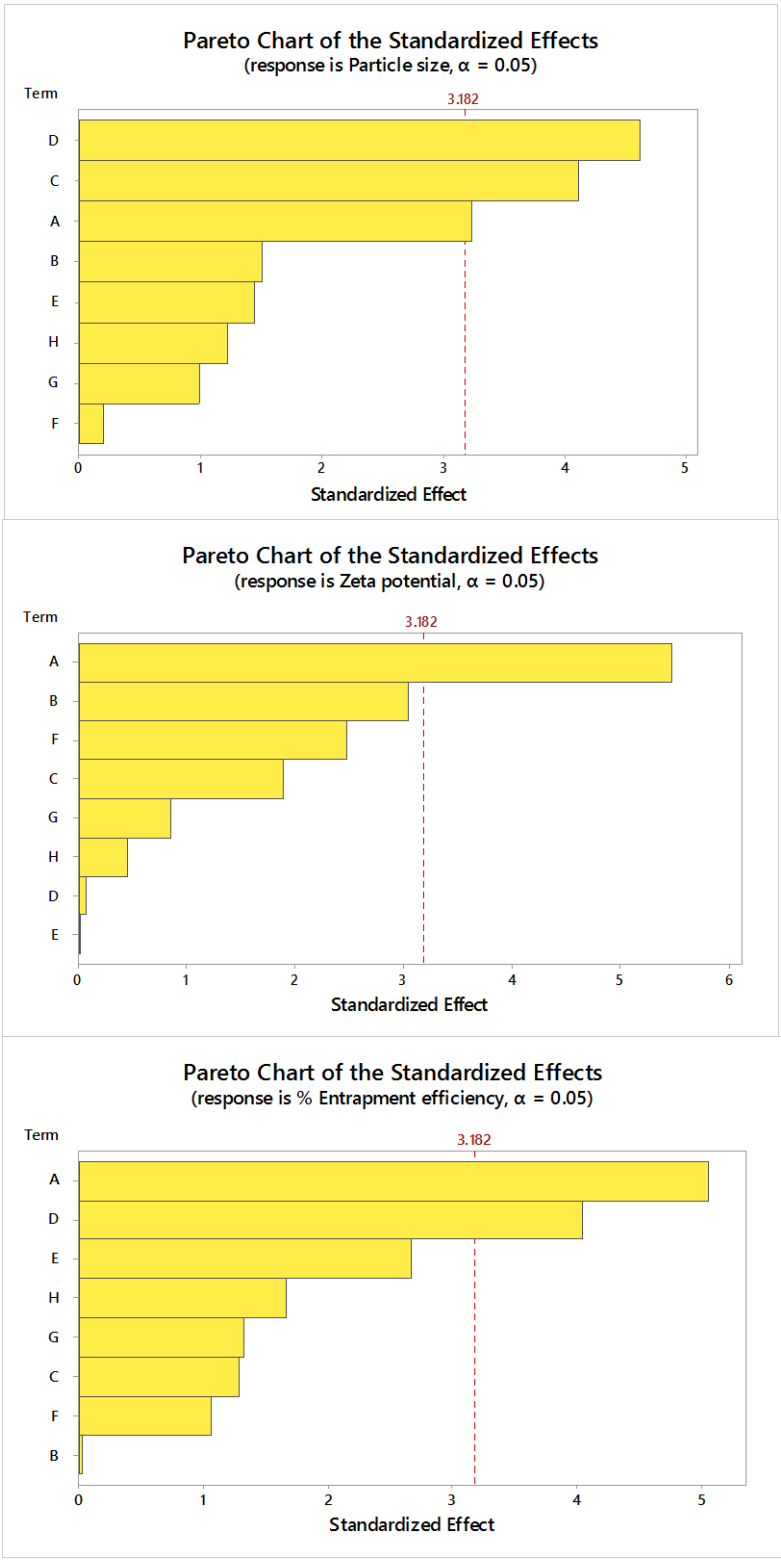

A - polymer concentration; B - stirring speed; C - stirring time; D - sonication time; E - sonication frequency; F - temperature; G - centrifugation time; H - centrifugation speed.

Figure 5.6 Pareto charts showing the influence of significant factors on responses

5.2.2 Box-Behnken experimental design

BBD was employed consisting of 3 factors, 3 levels and 3 center points (Table 5.6). The BBD design matrix comprised of 15 runs recognized by Minitab 17 software. ANOVA was performed in order to test the significance of all the coefficients and thereby to do away with the less significant factors. The generated quadratic equations for each response were denoted by '+' sign for synergistic effect and '-' sign for antagonistic effect. The effects on PS, % EE and ZP were showed, which were determined using Minitab 17 software (Table 5.7).

Table 5.6 Factors and responses with their levels in BBD

Factors	**Name**	**Unit**	**Min.**	**Max.**
X_1	Polymer concentration	% w/w	0.02	0.08
X_2	Stirring time	hours	4	6
X_3	Sonication time	mins	10	20
Responses	**Name**	**Unit**	**Constraint**	
Y_1	Particle size	nm	Minimize	
Y_2	% Entrapment efficiency	%	Maximize	
Y_3	Zeta potential	mV	Minimize	

Table 5.7 Compositions of the 3-factor 3-level BBD for the formulation of DSB-PVP-Ch-GNPs

Run	A	B	C	Y_1*	Y_2*	Y_3*
F1	0.05	5	15	32.40±1.22	-15.59±1.26	59.22±0.38
F2	0.05	5	15	32.34±1.28	-16.55±1.02	59.92±0.56
F3	0.02	4	15	30.19±1.46	-20.72±1.04	49.39±0.81
F4	0.02	5	20	27.86±1.62	-19.92±1.10	46.29±0.47
F5	0.05	4	20	34.98±1.21	-15.33±1.16	62.98±0.34
F6	0.08	5	10	34.46±1.29	-13.94±1.33	64.82±0.39
F7	0.05	6	10	29.52±1.34	-16.20±1.42	47.98±0.52
F8	0.02	6	15	24.33±1.62	-20.56±1.14	34.27±0.74
F9	0.05	4	10	34.92±1.42	-17.38±1.64	62.84±0.86
F10	0.08	6	15	31.89±1.12	-12.58±1.08	60.59±0.84
F11	0.05	5	15	32.29±1.08	-17.59±1.26	59.68±0.39
F12	0.08	4	15	36.14±1.28	-12.39±1.16	64.16±0.62
F13	0.08	5	20	34.39±1.24	-13.73±1.29	64.26±0.38
F14	0.05	6	20	29.31±1.56	-15.31±1.19	47.49±0.52
F15	0.02	5	10	27.82±1.48	-20.38±1.21	46.80±0.54

(* Mean ± SD, n = 3)

[A - polymer concentration; B - stirring time; C - sonication time; Y_1 - particle size; Y_2 - zeta potential; Y_3 - % entrapment efficiency].

5.2.2.1 Influence of the factors on PS

The mean PS of the DSB-PVP-Ch-GNPs according to the factorial design ranged between 24.33 ± 1.62 nm to 36.14 ± 1.28 nm. The following equation shows the relationship between the independent variables and PS:

$$Y_1 = 31.77 + 199.9\,A + 0.163\,B - 0.128\,C - 1531.0\,A^2 - 0.3279\,B^2 + 0.00668\,C^2 + 13.42\,AB - 0.183\,AC - 0.0135\,BC$$

The relationship between the independent variables and PS was further elucidated by 3-D response surface plots, and the corresponding graphs that evaluate the effects of factors on PS are shown in Figure 5.7. Statistical ANOVA analysis results of

the quadratic model generated for PS is given in Table 5.8. The quadratic model having *p*-value of <0.05 and F-value of 619.04 suggests that it was the best fit for PS. The R-sq value was found to be 99.91%, indicating a good fit between predicted and experimental values. The lack of fit was 0.065 implies that the quadratic model had no lack of fit (>0.05). Thus, this model could be used to navigate the design space and plot the response optimizer.

5.2.2.2 Influence of the factors on ZP

The ZP for DSB-PVP-Ch-GNPs according to the factorial design ranged between -12.39 ± 1.16 to -20.72 ± 1.04 mV. The following equation shows the relationship between the independent variables and ZP:

$Y_2 = 19.1 - 193\ A + 3.60\ B - 0.346\ C + 513\ A^2 - 0.476\ B^2 - 0.0018\ C^2 + 2.9\ AB + 0.42\ AC + 0.0580\ BC$

The relationship between the independent variables and ZP was further elucidated using 3-D response surface plots. The corresponding graphs that evaluate the effects of factors on ZP are shown in Figure 5.7. Statistical ANOVA analysis results of the quadratic model generated for ZP is given in Table 5.8. The quadratic model was found to be significant with p-value of <0.05 and F-value of 13.33 suggests that it was the best fit for ZP. The R-sq value was found to be 96.00%, indicating a good fit between predicted and experimental values. The lack of fit was 0.583 implies that the quadratic model had no lack of fit (>0.05). Thus, this model could be used to navigate the design space and plot the response optimizer.

5.2.2.3 Influence of the factors on % EE

The % EE for DSB-PVP-Ch-GNPs according to the factorial design ranged between 34.27 ± 0.74 % to 64.82 ± 0.39 %. The following equation shows the relationship between the independent variables and % EE:

$Y_3 = -26.9 + 290\ A + 34.90\ B - 0.084\ C - 1825\ A^2 - 4.362\ B^2 + 0.0031\ C^2 + 46.3\ AB + 3.25\ AC - 0.0315\ BC$

3-D response surface plots for the % EE of DSB-PVP-Ch-GNPs are shown in Figure 5.7. Statistical ANOVA analysis results of the quadratic model generated for % EE is given in Table 5.8. The quadratic model was found to be significant with p-value of <0.05 and F-value of 186.41 suggests that it was the best fit for entrapment efficiency. The R-sq value was found to be 99.70%, indicating a good fit between predicted and experimental values. The lack of fit was 0.081 implies that the quadratic model had no lack of fit (>0.05). Thus, this model could be used to navigate the design space and plot the response optimizer.

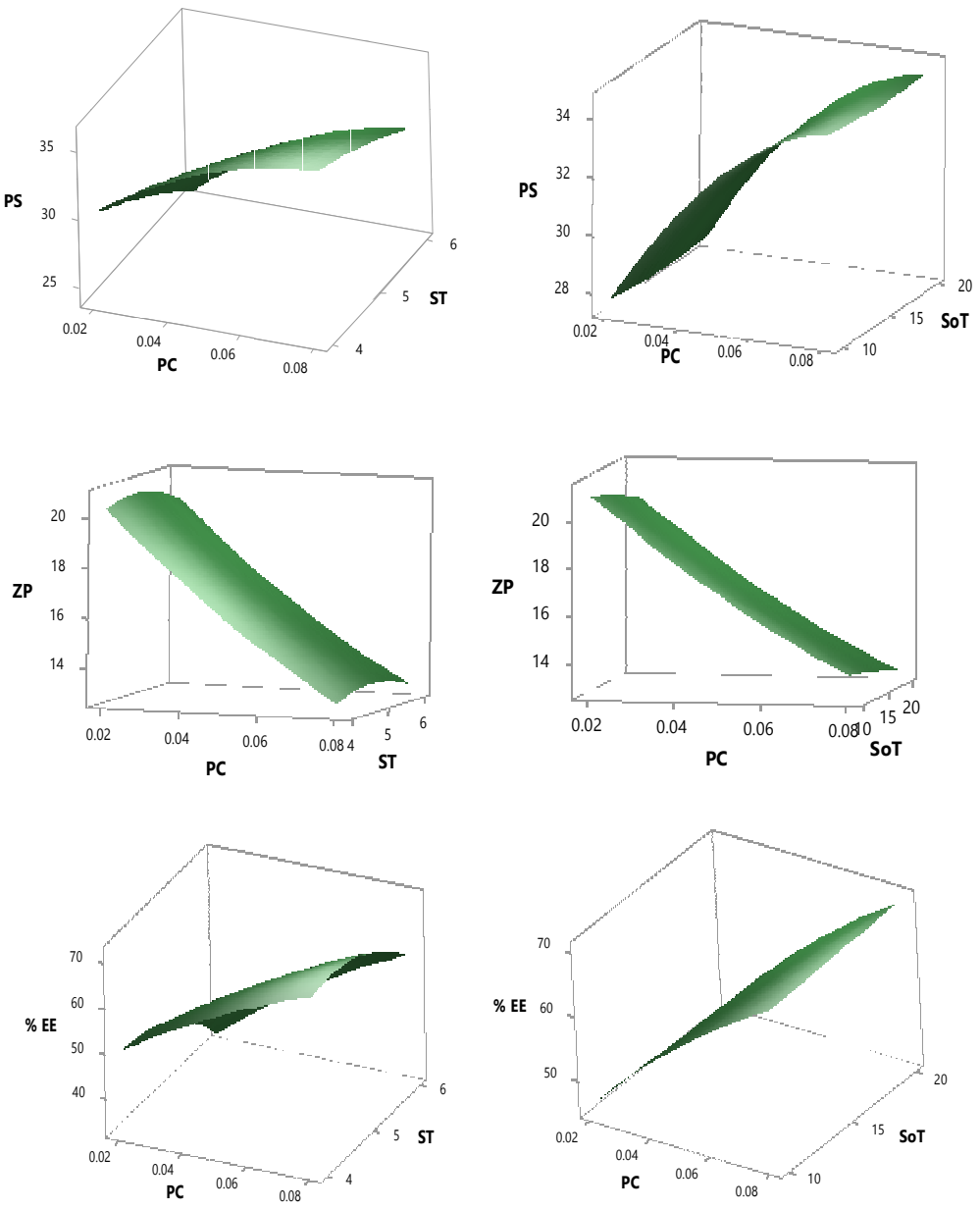

PS - particle size, % EE - entrapment efficiency, ZP - zeta potential, PC - polymer concentration, ST - stirring time and SoT - sonication time

Figure 5.7 3-D Response surface plots showing effect of polymer concentration, stirring time and sonication time on particle size, zeta potential and % entrapment efficiency

3-D response surface plot was generated in order to enumerate the interaction and correlation between the factors and measured responses. Significant *p*-value and lack of fit for all responses were revealed by statistical analysis of the quadratic model (Table 5.8) [Beg et al., 2013].

Table 5.8 Statistical ANOVA results of the quadratic model

Quadratic model							
Response	**F-value**	**p-value**	**R-sq**	**R-sq (adj)**	**R-sq (pred)**	**Lack of fit**	**Remarks**
PS	619.04	0.000	99.91%	99.75%	98.62%	0.065	Significant
ZP	13.33	0.005	96.00%	88.80%	60.31%	0.583	Significant
% EE	186.41	0.000	99.70%	99.17%	95.47%	0.081	Significant

PS - particle size, ZP - zeta potential and % EE - % entrapment efficiency

To attain a better formulation with appropriate PS, % EE and ZP, response optimization was performed. The optimum values were defined as 0.08 % w/w, 6 hours and 19.70 mins for the PC, ST and SoT, respectively. PS, ZP and % EE were predicted as 30.90 nm, -14.08 mV and 61.02 %, respectively (Table 5.9).

Table 5.9 Results of optimization of DSB-PVP-Ch-GNPs utilizing BBD

Factors for response optimization		
A – Polymer concentration (% w/w)	0.08	
B – Stirring time (hours)	6	
C – Sonication time (minutes)	19.70	
Optimized results		
Responses	**Predicted value**	**Experimental value***
Y_1 – Particle size (nm)	31.76	30.90 ± 1.14
Y_2 – Zeta potential (mV)	-12.75	-14.08 ± 1.02
Y_3 – Entrapment efficiency (%)	60.19	61.02 ± 0.39

(* Mean ± SD, n = 3)

5.2.3 FTIR and XRD studies

The FTIR spectral study was performed to examine the DSB interaction with other components used in the formulation. The overlay spectrum of DSB, PVP, Ch, Ch-GNP, and DSB-PVP-Ch-GNPs is presented in Figure 5.8. The FTIR spectrum of DSB showed its characteristic peaks at 773.48 cm^{-1} (C-Cl), 1577.82 cm^{-1} (-C-H, CH=CH), 1620.26 cm^{-1} (C=O stretching), 2949.26 cm^{-1} (C-H stretching), 3061.13 cm^{-1} (-C-H

aromatic ring), 3201.94 cm^{-1} (O-H stretching), and 3412.19 cm^{-1} (N-H stretching). For PVP the peaks appeared were 3436.62 cm^{-1} (O-H stretching), 2950.47 cm^{-1} (C-H stretching), 1652.78 cm^{-1} (C=O stretching), 1428.54 cm^{-1} (CH_2 bending) and 1240.97 cm^{-1} (C-N). All the characteristic peaks pertaining to DSB were retained in the FTIR spectrum of the DSB-PVP-Ch-GNPs, confirming the non-interaction of DSB with other components and there was no change in its chemical nature during the preparation process.

The overlay XRD spectrum of DSB, PVP, Ch, Ch-GNPs and DSB-PVP-Ch-GNPs is presented in Figure 5.8. The peaks that were observed were well resolved and intense for pure DSB, demonstrating the crystalline nature of DSB. The diffraction patterns of the PVP, Ch and Ch-GNPs showed various small diffuse peaks with the broad halo. The XRD spectrum of the DSB-PVP-Ch-GNPs exhibited broad diffuse peaks resulting in the decrease in the crystalline nature of the DSB, suggesting that DSB had been converted into amorphous nature.

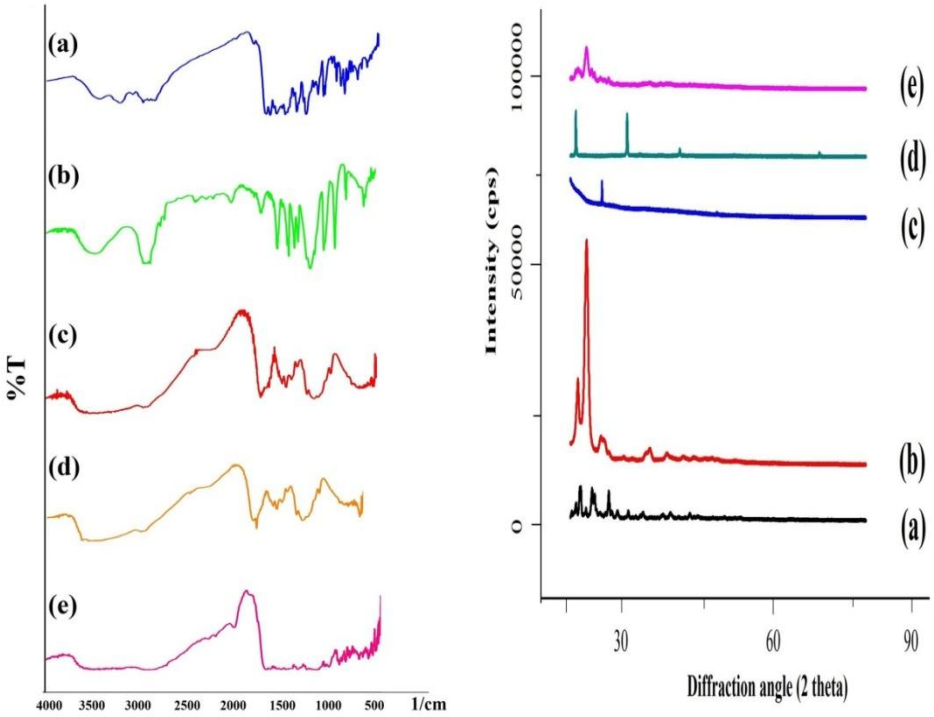

(a) DSB, (b) PVP, (c) Ch, (d) Ch-GNPs and (e) DSB-PVP-Ch-GNPs.

(A) **(B)**

Figure 5.8 Fourier transform infrared overlay spectrum (A) and x-ray diffraction overlay spectrum (B)

5.2.4 TEM

TEM analysis was performed to determine the surface morphology of DSB-PVP-Ch-GNPs. The study revealed that the DSB-PVP-Ch-GNPs were spherical in shape having uniform size distribution. At different magnifications, they appeared as spherical particles having a smooth surface without any ruptures and a dark inner core and a lighter outer envelop. Due to the difference in the electron density between the gold core and outer envelop, a clear core-shell structure of DSB-PVP-Ch-GNPs is visible (Figure 5.9).

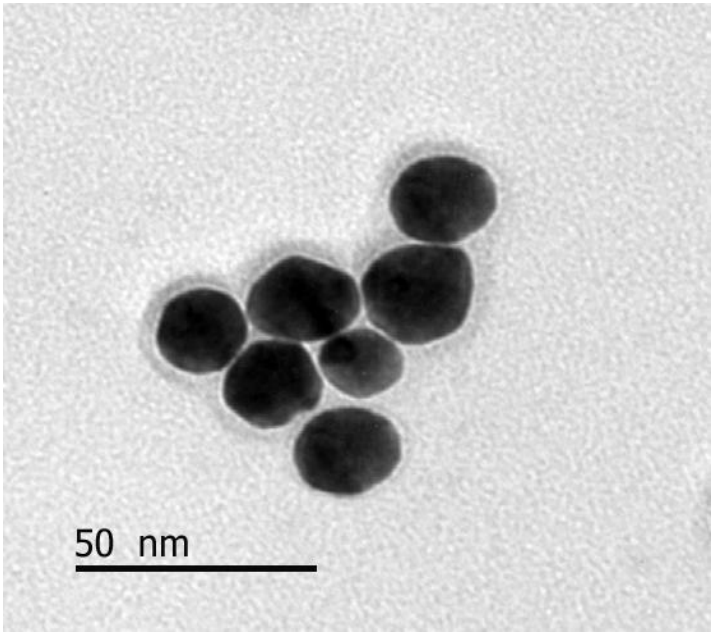

Figure 5.9 Transmission electron microscopy micrograph of DSB-PVP-Ch-GNPs

5.2.5 *In vitro* drug release study

The capacity of the drug carrier to efficiently release the therapeutic payload at the absorption or the desired site is a prerequisite requirement for any delivery vehicle. DSB release pattern out of DSB-PVP-Ch-GNPs was studied in pH 7.4 phosphate buffer at 37 ± 0.5^0 C for 48 hours (Figure 5.10). Approximately 25 % of DSB was released in the first 4 hours, and total 69 % of DSB was released at the end of 48 hours, indicating sustained drug release pattern which is likely due to the strong interaction between DSB/PVP/Ch-GNP conjugates.

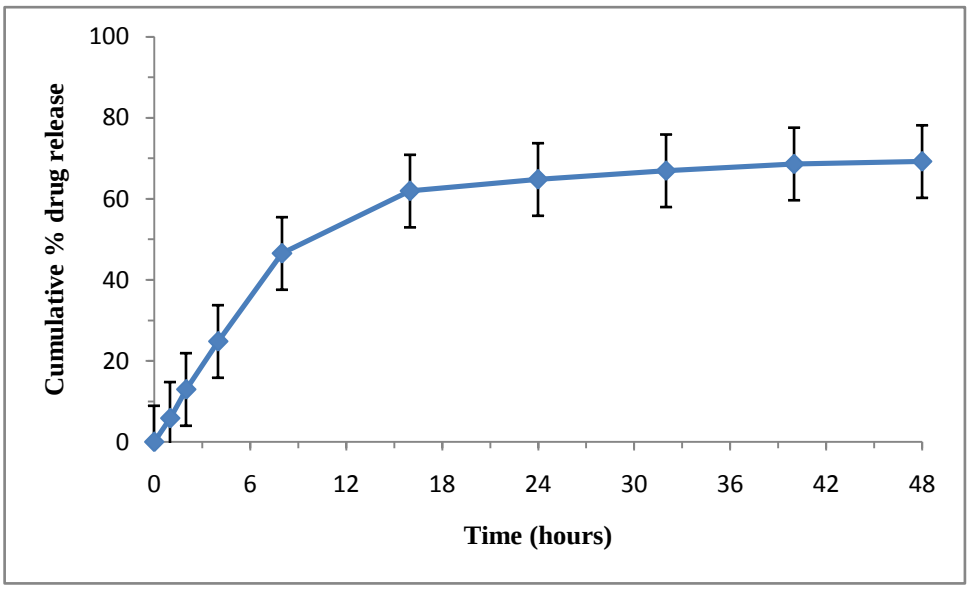

(vertical bars represents mean ± SD and n = 3)

Figure 5.10 *In vitro* drug release profile of the optimized DSB-PVP-Ch-GNPs nanoformulation in pH 7.4 phosphate buffer

5.3 Preparation of DSB loaded PEG stabilized chitosan capped GNPs (DSB-PEG-Ch-GNPs)

The synthesized Ch-GNPs were visually observed for the appearance of any color change in the dispersion. A clear deep ruby red color was formed within 1 hour, as a result of bioreduction by chitosan which indicated the green synthesis of Ch-GNPs and the dispersion was examined by UV-Visible spectrophotometry. The dispersion was scanned in the range of 300-800 nm wavelength. In the UV–Vis absorption spectrum, a peak maximum at 525 nm was recorded, which is attributed to the SPR band of GNPs. After the successful synthesis of Ch-GNPs, subsequent stabilization and loading of DSB were done.

5.3.1 Risk assessment studies

The identification of CQAs that might influence the quality of the nanoformulation is a prerequisite of QbD. The essential CQAs were prioritized by FMEA based on rank modes of relative effectiveness as low, medium and high. The

results obtained by employing DOE to optimize the GNPs manufacturing process were further subjected to screening design.

5.3.2 Optimization process variables by PBD and BBD

Through preliminary screening experiments by employing PBD, PC, ST and SoT were identified as the most significant variables within the range of 0.01-0.10 % w/w, 4-8 hours, 10-30 mins, respectively. 12 experimental runs were generated in PBD from 8 factors, 3 responses, and 2 levels (Table 5.10). The statistical evaluation was conducted by applying ANOVA, and then Pareto charts were generated in order to screen out the significant factors influencing the responses (Figure 5.11).

Table 5.10 Plackett-Burman screening design of experiment and their results

Run	A	B	C	D	E	F	G	H	Y_1*	Y_2*	Y_3*
PB-1	-	+	-	-	-	+	+	+	29.35±0.53	42.56±0.36	-17.08±0.08
PB-2	+	-	+	-	-	-	+	+	31.64±0.61	65.16±0.28	-10.20±0.06
PB-3	+	+	+	-	+	+	-	+	28.85±0.82	54.86±0.22	-13.07±0.11
PB-4	-	-	-	-	-	-	-	-	34.11±0.58	51.28±0.18	-12.11±0.10
PB-5	-	-	+	+	+	-	+	+	14.66±0.70	59.19±0.27	-14.77±0.07
PB-6	+	-	-	-	+	+	+	-	32.45±0.65	59.74±0.29	-11.90±0.13
PB-7	-	+	+	-	+	-	-	-	16.31±0.68	40.11±0.18	-16.50±0.10
PB-8	-	+	+	+	-	+	+	-	12.20±0.76	69.31±0.16	-17.44±0.09
PB-9	+	+	-	+	+	-	+	-	24.19±0.55	72.10±0.24	-11.21±0.06
PB-10	+	+	-	+	-	-	-	+	27.22±0.64	75.35±0.21	-11.36±0.14
PB-11	+	-	+	+	-	+	-	-	21.18±0.73	77.54±0.26	-12.67±0.09
PB-12	-	-	-	+	+	+	-	+	23.39±0.79	40.51±0.19	-13.61±0.12

(Note: + high level, - low level; * Mean ± SD, n = 3)

[A-polymer concentration; B-stirring speed; C-stirring time; D- sonication time; E-sonication frequency; F-temperature; G- centrifugation time; H-centrifugation speed.; Y_1-particle size; Y_2- % entrapment efficiency; Y_3-zeta potential].

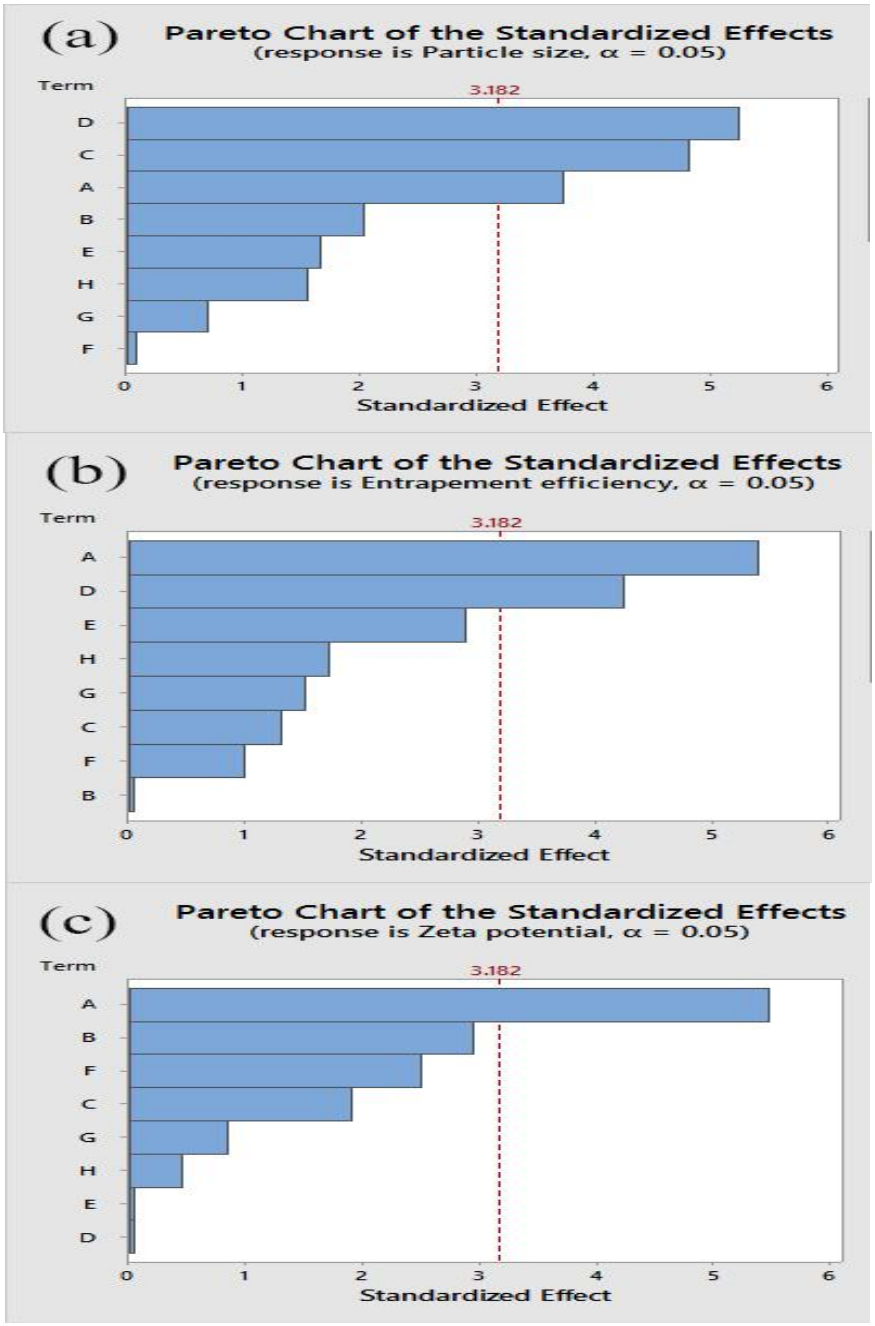

A-polymer concentration; B-stirring speed; C-stirring time; D- sonication time; E-sonication frequency; F-temperature; G- centrifugation time; H-centrifugation speed.

Figure 5.11 Pareto chart showing the influence of factors on responses; (a) influence of input factors on PS, (b) influence of input factors on %EE and (c) influence of input factors on ZP

3 factor, 3 level and 3 center point BBD was employed (Table 5.11). The design matrix comprised of 15 runs recognized by Minitab 17 software. In order to test the significance of all coefficients, ANOVA was performed. The quadratic equations were generated for each response which is denoted by '+' sign for synergistic effect and '-'

sign for antagonistic effect. The effects on particle size, entrapment efficiency, and zeta potential were showed (Table 5.12).

Table 5.11 Factors and responses with their levels in BBD

Levels			
Independent variables (Factors)	**Low (-1)**	**Medium (0)**	**High (+1)**
A. Polymer concentration (% w/w)	0.010	0.055	0.100
B. Stirring time (hours)	4	6	8
C. Sonication time (mins)	10	20	30
Dependent variables (Responses)		**Constraint**	
Y_1 = Particle size (nm)		Minimize	
Y_2 = Entrapment efficiency (%)		Maximize	
Y_3 = Zeta potential (mV)		Minimize	

Table 5.12 Compositions of the 3-factor 3-level BBD for the formulation of DSB-PEG-Ch-GNPs

Run	**A**	**B**	**C**	**Y_1***	**Y_2***	**Y_3***
F1	0.100	4	20	32.19±1.52	77.11±0.84	-10.31±1.08
F2	0.100	8	20	27.96±1.38	67.62±0.78	-10.68±1.12
F3	0.100	6	30	30.36±1.46	77.13±0.82	-11.68±1.19
F4	0.055	8	30	25.38±1.81	54.56±0.88	-13.29±1.16
F5	0.010	6	30	23.96±1.50	53.33±0.79	-17.89±1.14
F6	0.055	6	20	28.34±1.36	66.29±0.76	-13.65±1.09
F7	0.010	6	10	23.92±1.48	53.73±0.86	-18.43±1.13
F8	0.010	8	20	20.23±1.61	41.22±0.83	-18.54±1.10
F9	0.055	8	10	25.41±1.84	54.97±0.93	-14.12±1.16
F10	0.100	6	10	30.38±1.45	75.60±0.80	-11.88±1.07
F11	0.010	4	20	26.38±1.39	56.68±0.86	-18.69±1.11
F12	0.055	6	20	28.30±1.53	66.72±0.91	-15.62±1.14
F13	0.055	4	10	30.86±1.48	69.49±0.79	-15.44±1.17
F14	0.055	4	30	30.88±1.94	69.61±0.81	-13.27±1.09
F15	0.055	6	20	28.31±1.56	66.85±0.87	-14.62±1.13

(* Mean ± SD, n = 3)
[A - polymer concentration (% w/w); B - stirring time (hour); C - sonication time (min); Y_1 - particle size (nm); Y_2 - entrapment efficiency (%); Y_3 - zeta potential (mV)].

5.3.2.1 Influence of factors on PS, ZP and % EE

The mean PS of the DSB-PEG-Ch-GNPs fabricated according to the factorial design ranged between 20.23 ± 1.61 nm to 32.19 ± 1.52 nm. The following equation shows the relationship between the factors and PS:

$Y_1 = +29.623 + 112.73A - 0.640B - 0.0505C - 643.0A^2 - 0.0811B^2 + 0.001404C^2 + 5.333\ AB - 0.033AC - 0.00063BC$

PS was mainly affected by the polymer concentration (A). A positive correlation was observed between polymer concentration and particle size, such that PS increased with increase in polymer concentration. Contour and 3D response surface plots were generated to elucidate the relationship between the factors and PS. The corresponding graphs that evaluate the effects of factors on PS are shown in Figure 5.12 (A-D). Statistical ANOVA analysis results of PS were given in Table 5.13. This model was found to be significant (F-value = 847.42; *p*-value <0.05; R-sq value = 99.93%), the predicted and experimental values were in reasonable agreement and thus the design space could be navigated.

The % EE for DSB-PEG-Ch-GNPs fabricated according to the factorial design ranged between 41.22 ± 0.83% to 77.13 ± 0.82%. The impact of polymer concentration was more prominent than the effects of the stirring time (B) and sonication time (C). The following equation shows the relationship between the factors and % EE:

$Y_2 = +36.49 + 222.7\ A + 8.93\ B + 0.028\ C - 783\ A^2 - 1.093\ B^2 - 0.00091\ C^2 + 16.53\ AB + 1.061\ AC - 0.0066\ BC$

According to Figure 5.12 (E and F), at high polymer concentration and low stirring time, % EE improved by up to 77.13 ± 0.82%. Increasing the stirring time and

reducing the sonication time, initiated a decrease in % EE below 54.97 ± 0.93%. In the intermediate stirring time and high sonication time, % EE showed maximum values. Figure 5.12 (G and H) shows with the higher polymer concentration and sonication time, % EE increased up to 77.13 ± 0.82%. According to the results, the % EE was enhanced with an increase in the polymer concentration, stirring time and sonication time. Statistical ANOVA analysis results of % EE were given in Table 5.13. This model was found to be significant (F-value = 261.87; *p*-value <0.05; R-sq value = 99.79%), the predicted and experimental values were in reasonable agreement and thus the design space could be navigated.

The ZP for DSB-PEG-Ch-GNPs fabricated according to the factorial design ranged between -10.31 ± 1.08 to -18.69 ± 1.11 mV. The following equation shows the relationship between the factors and ZP:

$Y_3 = -18.80 + 116.5\ A - 1.04\ B + 0.121\ C - 214\ A^2 + 0.127\ B^2 + 0.00093\ C^2 - 1.44\ AB - 0.19\ AC - 0.0167\ BC$

According to Figure 5.12 (I and J), an increase in the polymer concentration resulted in ZP increase, which may be due to the effect of the change in the plane of shear away from the surface of the particle. Statistical ANOVA analysis results of ZP were given in Table 5.13. This model was found to be significant (F-value = 13.87; *p*-value <0.05; R-sq value = 96.15%), the predicted and experimental values were in reasonable agreement thus the design space could be navigated.

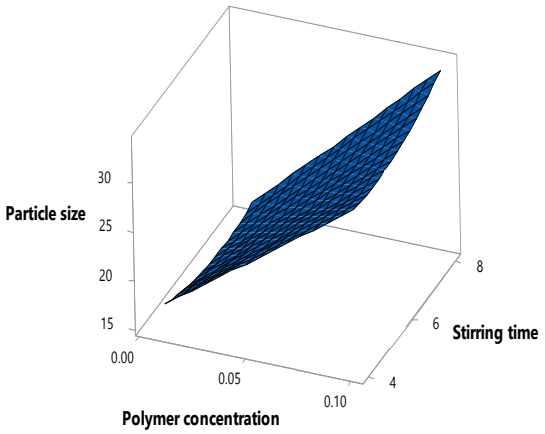
Particle size
30
25
20
15
0.00
0.05
0.10
Polymer concentration
4
6
8
Stirring time

(A)

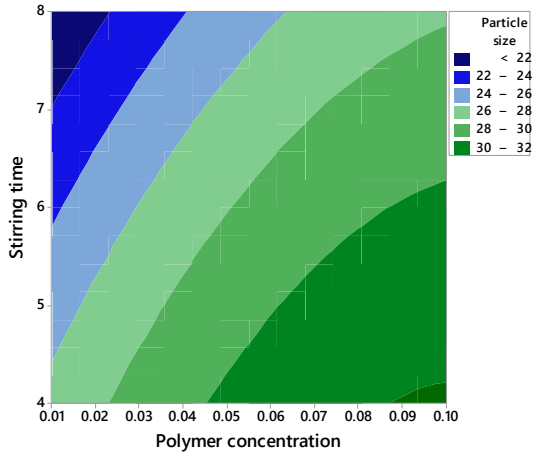
Particle size
< 22
22 – 24
24 – 26
26 – 28
28 – 30
30 – 32
Stirring time
8
7
6
5
4
0.01 0.02 0.03 0.04 0.05 0.06 0.07 0.08 0.09 0.10
Polymer concentration

(B)

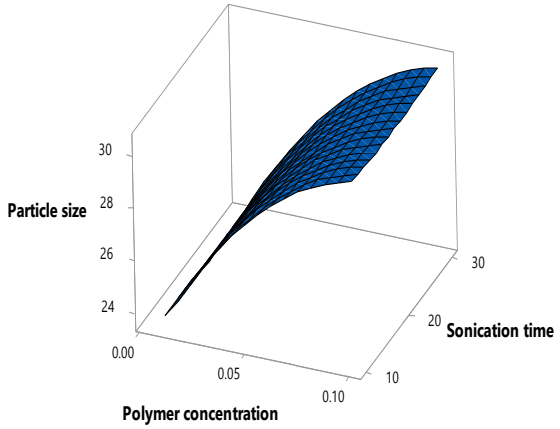
Particle size
30
28
26
24
0.00
0.05
0.10
Polymer concentration
10
20
30
Sonication time

(C)

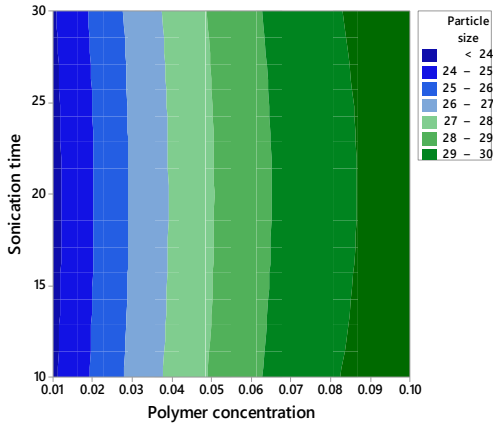
Particle size
< 24
24 – 25
25 – 26
26 – 27
27 – 28
28 – 29
29 – 30
Sonication time
30
25
20
15
10
0.01 0.02 0.03 0.04 0.05 0.06 0.07 0.08 0.09 0.10
Polymer concentration

(D)

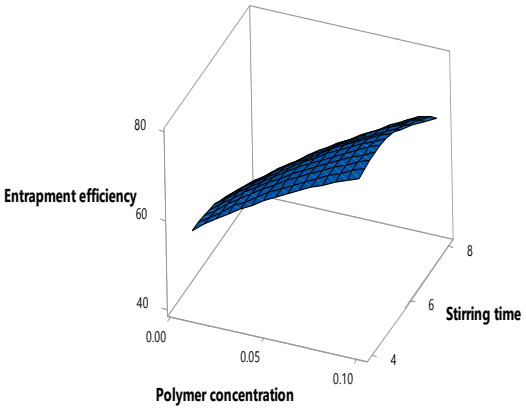
Entrapment efficiency
80
60
40
0.00
0.05
0.10
Polymer concentration
4
6
8
Stirring time

(E)

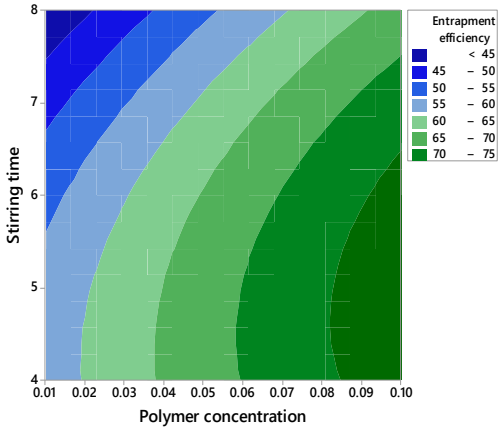
Entrapment efficiency
< 45
45 – 50
50 – 55
55 – 60
60 – 65
65 – 70
70 – 75
Stirring time
8
7
6
5
4
0.01 0.02 0.03 0.04 0.05 0.06 0.07 0.08 0.09 0.10
Polymer concentration

(F)

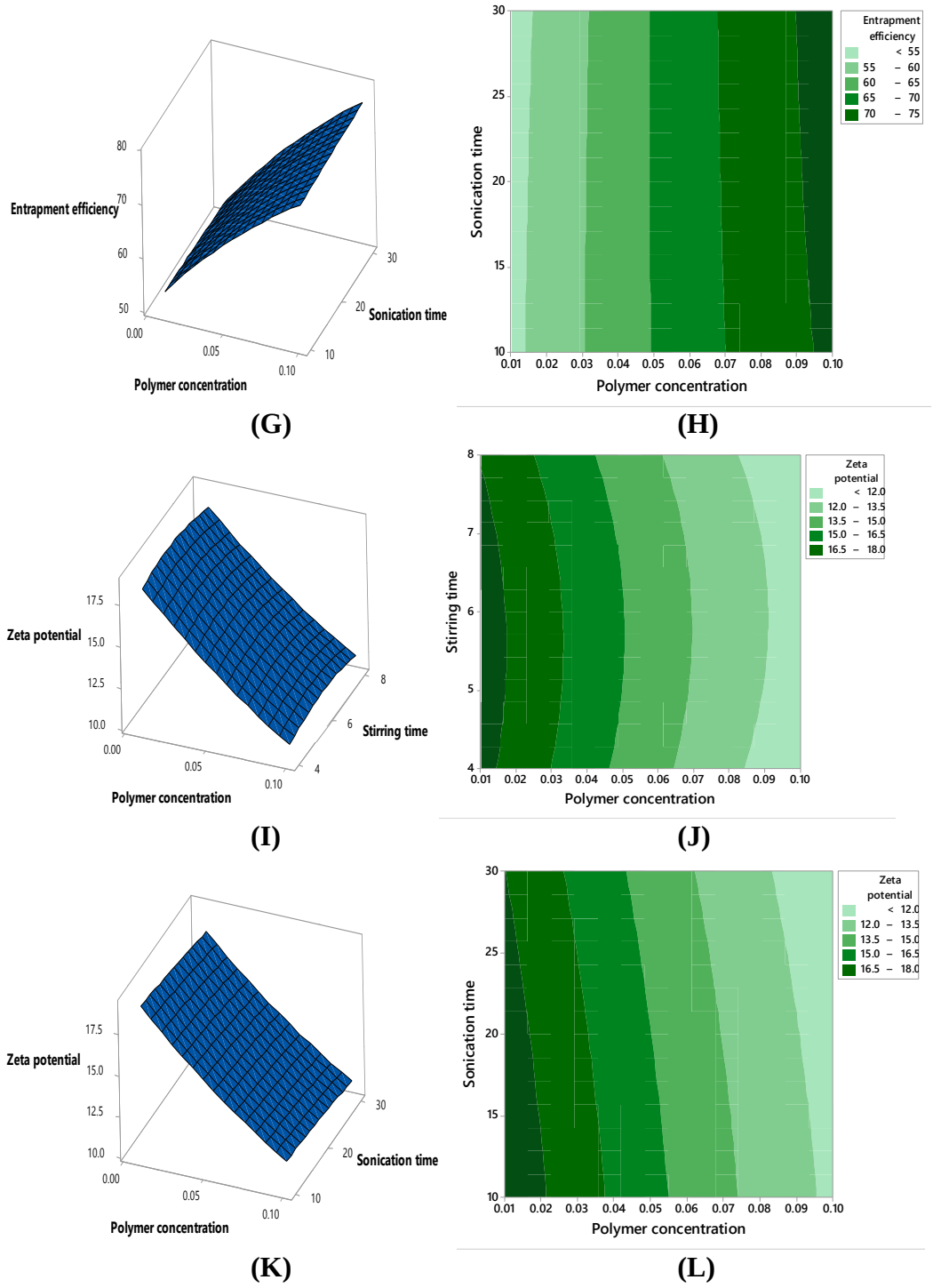

Figure 5.12 Graphical illustration representing the effect of factors on responses. (A & C) represents 3-D response surface plots of PS, (B & D) are its contour plots; (E & G) represents 3-D response surface plots of % EE, (F & H) are its contour plots; (I & K) represents 3-D response surface plots of ZP, (J & L) are its contour plots

3-D response surface and contour plots were created in order to enumerate the interaction and correlation between the factors and measured responses. Significant *p*-

value and lack of fit for all responses were revealed by statistical analysis of the quadratic model (Table 5.13)

Table 5.13 Statistical ANOVA results of the quadratic model

Quadratic model							
Response	**F-value**	**p-value**	**R-sq**	**R-sq (adj)**	**R-sq (pred)**	**Lack of fit**	**Remarks**
PS	847.42	0.000	99.93%	99.82%	98.96%	0.063	Significant
% EE	261.87	0.000	99.79%	99.41%	96.77%	0.078	Significant
ZP	13.87	0.005	96.15%	89.21%	61.83%	0.584	Significant

PS - particle size, % EE - % entrapment efficiency, ZP - zeta potential.

5.3.2.2 Formulation optimization for the DSB-PEG-Ch-GNPs

In order to achieve an improved formulation with appropriate PS, % EE and ZP, response optimization was performed. Optimization plot with desired PS, % EE and ZP is illustrated in Figure 5.13. The optimum points were defined as 0.10 % w/w, 8 hours and 26.16 mins for the polymer concentration, stirring time and sonication time, respectively. PS, % EE and ZP were predicted as 27.84 nm, 67.13 % and -10.86 mV, respectively (Table 5.14) and their % biasness was found to be < 2 which was further validated and reported.

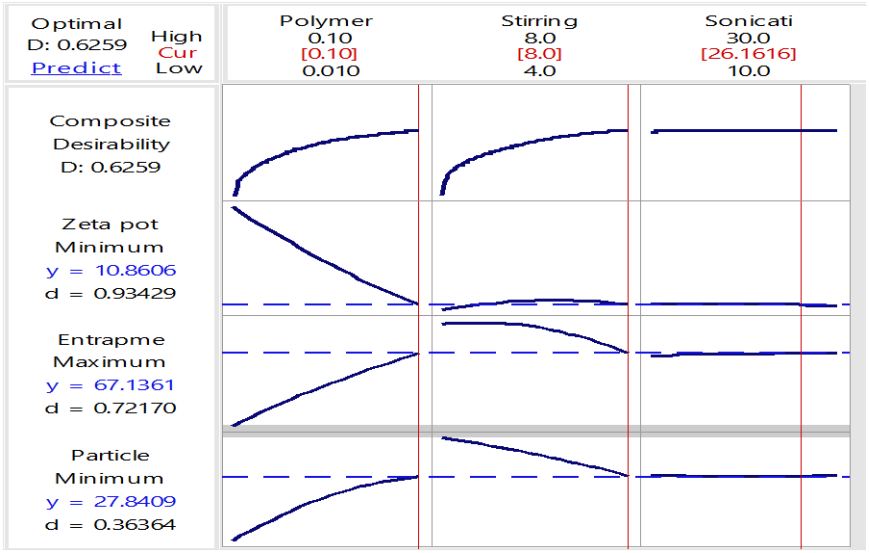

Figure 5.13 Optimization plot to prepare the formulation with desired PS, % EE and ZP

Table 5.14 Results of optimization of DSB-PEG-Ch-GNPs utilizing BBD

Independent variables for response optimization		
A – Polymer concentration (% w/w)	0.10	
B – Stirring time (hours)	8	
C – Sonication time (minutes)	26.16	
Optimized results		
Dependent variables (Responses)	**Predicted value**	**Experimental value***
Y_1 – Particle size (nm)	27.84	24.39 ± 1.82
Y_2 – Entrapment efficiency (%)	67.13	72.06 ± 0.86
Y_3 – Zeta potential (mV)	-10.86	-13.91 ± 1.21

(* Mean ± SD, n = 3)

5.3.3 Solid state characterization of DSB-PEG-Ch-GNPs

The overlay FTIR spectrum of DSB, PEG, Ch, Ch-GNP, and optimized DSB-PEG-Ch-GNPs is presented in Figure 5.14 (A). The FTIR spectrum of DSB showed its characteristic peaks at 3412.19 cm^{-1} (N-H stretching), 3201.94 cm^{-1} (O-H stretching), 3061.13 cm^{-1} (-C-H aromatic ring), 2949.26 cm^{-1} (C-H stretching), 1620.26 cm^{-1} (C $=$O stretching), 1577.82 cm^{-1} (-C-H, CH$=$CH) and 773.48 cm^{-1} (C-Cl). In the case of chitosan characteristic peaks were 1560.46 cm^{-1} (N-H), 1321.28 cm^{-1} (C-H), 1654.98 cm^{-1} (–NH2), 3390.97 cm^{-1} (-N-H) and 1031.95 cm^{-1} (C-O stretching). For PEG the peaks appeared were 3456.65 cm^{-1} (O-H stretching), 2850.88 cm^{-1} (C-H stretching), 1342.50 cm^{-1} (C–H bending), 1280.78 cm^{-1} (OH and C-O-H) and 1109.11 cm^{-1} (C-O-C). All the peaks that are characteristic of DSB were present in the FTIR spectrum of the optimized DSB-PEG-Ch-GNPs, confirming the non-interaction of DSB with other components.

Figure 5.14 (B) exhibited overlay XRD spectrum of DSB, PEG, Ch, Ch-GNPs, and optimized DSB-PEG-Ch-GNPs. The XRD spectrum of DSB exhibited sharp peaks at 2θ angles of 20.26^0, 21.11^0, 21.85^0, 24.41^0, 24.91^0, 27.07^0, 28.40^0, 29.50^0 and numerous minor peaks up to 30^0. The peaks that were observed were well resolved and intense, demonstrating the crystalline nature of DSB. The diffraction patterns of the

PEG, Ch and Ch-GNPs showed various minute diffuse peaks. The optimized DSB-PEG-Ch-GNPs showed broad diffuse peaks resulting in the decrease in the crystalline nature of the DSB, which suggests that the DSB had been converted into amorphous nature in the optimized nanoformulation.

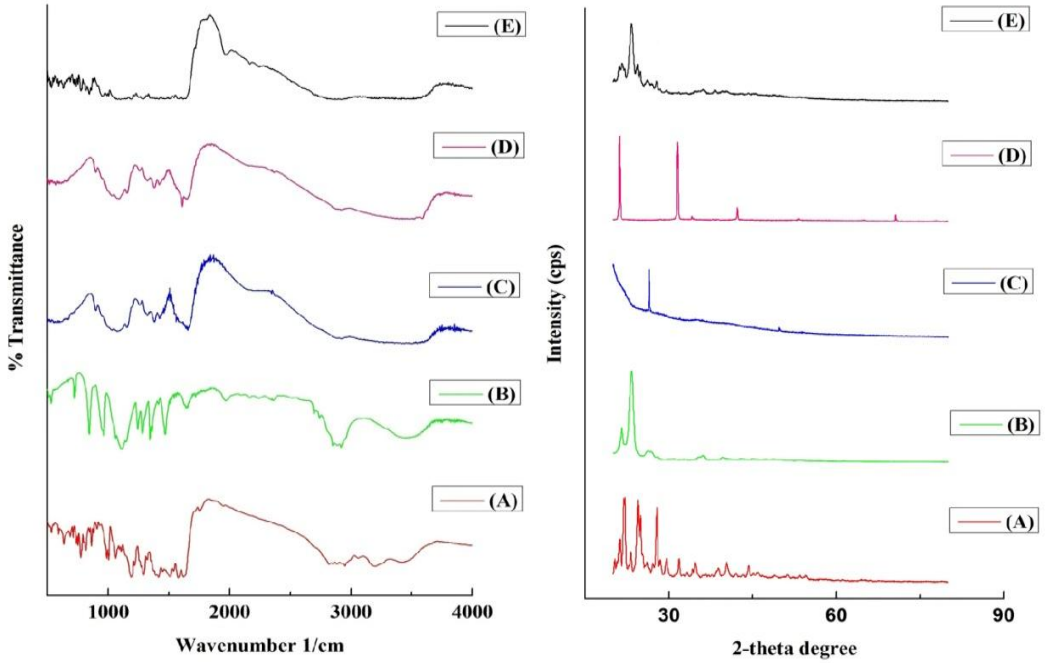

(A) DSB, (B) PEG, (C) Ch, (D) Ch-GNPs and (E) optimized DSB-PEG-Ch-GNPs

(A) **(B)**

Figure 5.14 Fourier transform infrared overlay spectrum (A) and x-ray diffraction overlay spectrum (B)

5.3.4 Physicochemical and morphological characterization

The grains of optimized DSB-PEG-Ch-GNPs were primarily spherical, having gold in the core (Figure 5.15). As the optimized DSB-PEG-Ch-GNPs were in the nanoscale size of around 25 nm, no clear differences in the size or shape could be observed due to the limitation of the resolution. For this purpose, TEM was employed.

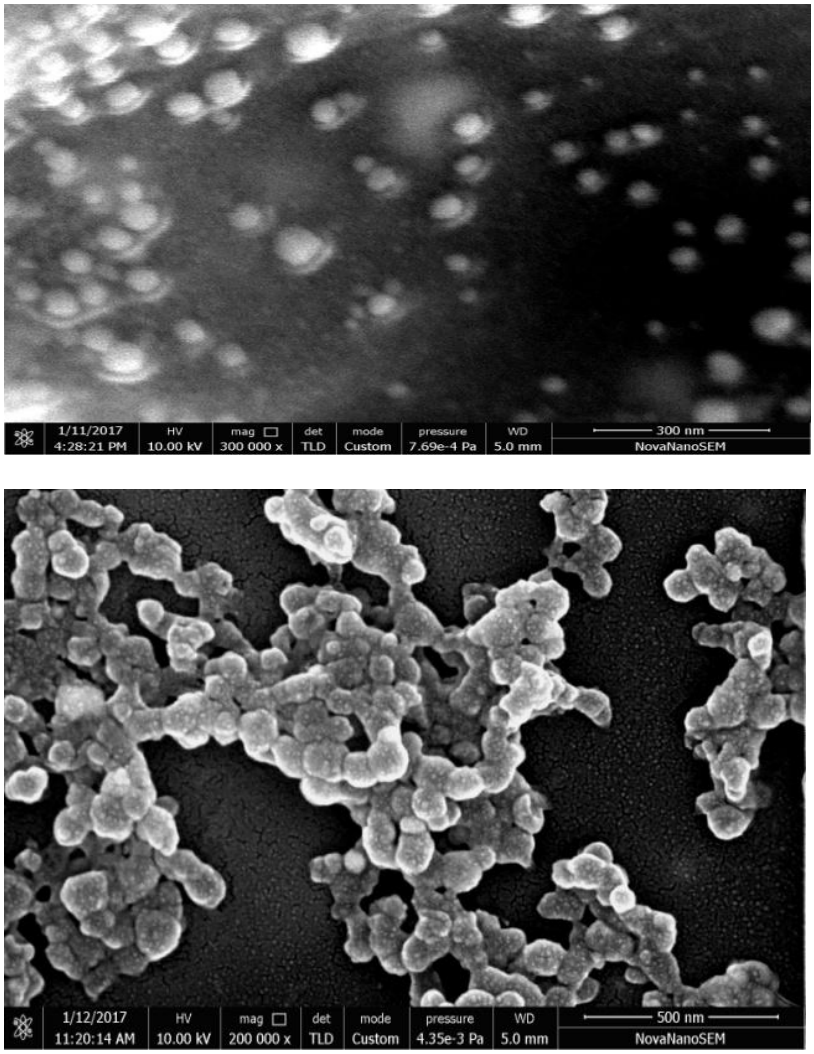

Figure 5.15 High resolution scanning electron microscopy micrographs showing the morphology of optimized DSB-PEG-Ch-GNPs

In the EDXS spectrum, clear and sharp peaks of gold (Au) were observed, confirming the successful reduction of the GNPs precursor (Figure 5.16 (A)). Besides Au peaks, signals for carbon (C) and other atoms were indicated by the weaker signals, which may be due to the adherence of biomolecules that were used in the synthesis of GNPs. The copper (Cu) peaks likely originated from the copper grid, onto which the optimized DSB-PEG-Ch-GNPs was placed. The color mapping report of the relative distribution of Au in the densely occupied region of optimized DSB-PEG-Ch-GNPs is shown in Figure 5.16 (B).

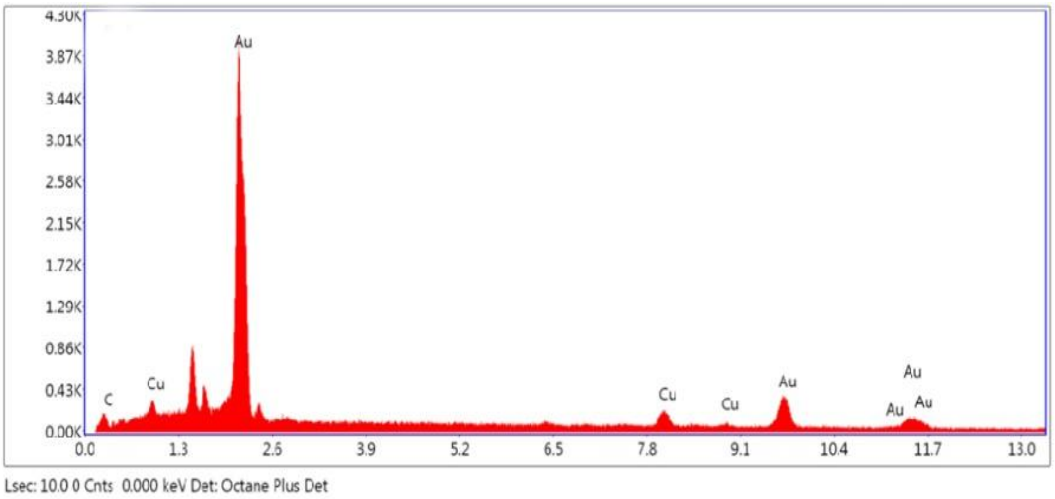

(A)

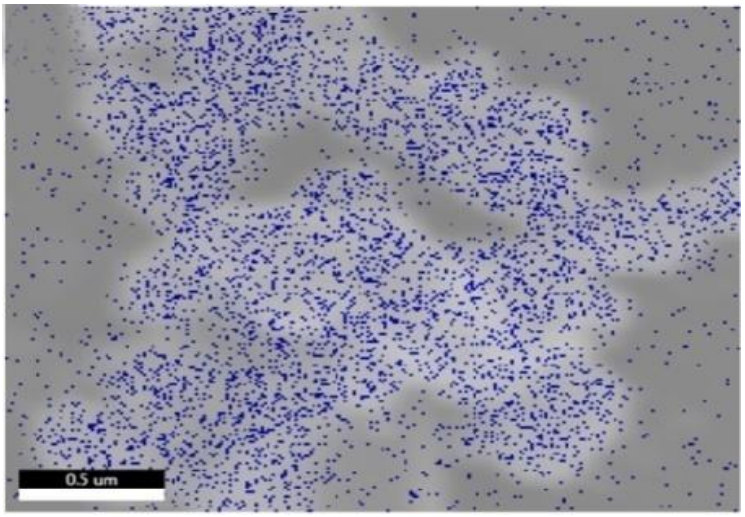

(B)

Figure 5.16 Energy dispersive x-ray spectroscopy spectrum of the optimized DSB-PEG-Ch-GNPs (A) and color mapping report of the relative distribution of Au in the optimized DSB-PEG-Ch-GNPs (B)

TEM analysis revealed that the optimized DSB-PEG-Ch-GNPs were spherical in shape having uniform size distribution. At different magnifications, they appeared as spherical particles having a smooth surface without any ruptures and a dark inner core and a lighter outer envelop. Due to the difference in the electron density between the gold core and outer envelop, a clear core-shell structure of DSB-PEG-Ch-GNPs is visible (Figure 5.17).

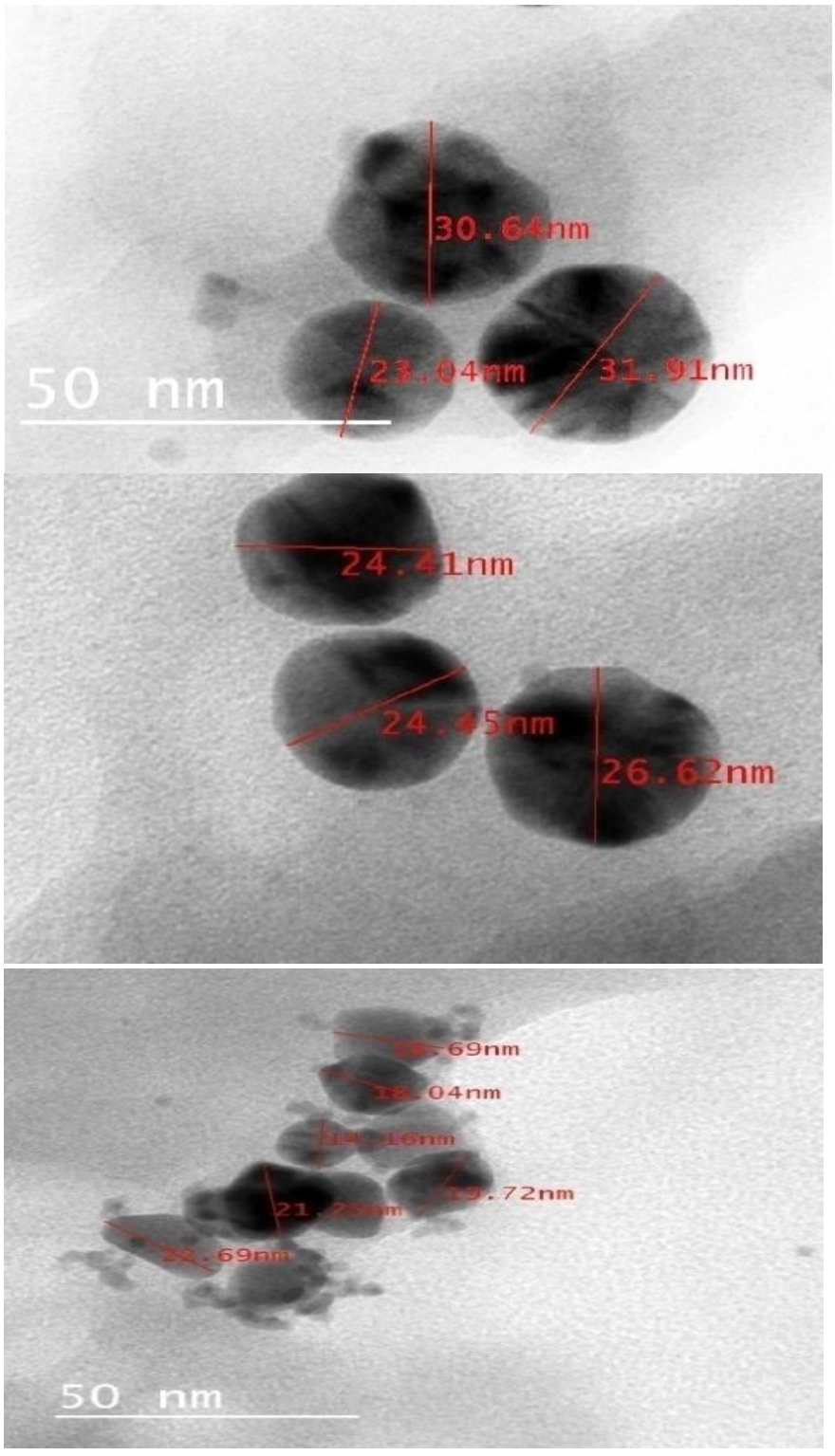

Figure 5.17 Transmission electron microscopy micrographs illustrating the shape and morphology of optimized DSB-PEG-Ch-GNPs

The SAED pattern of the spherical optimized DSB-PEG-Ch-GNPs showed bright circular spots confirming the presence of gold and the diffuse halo was indicative of scattering from an amorphous material (Figure 5.18).

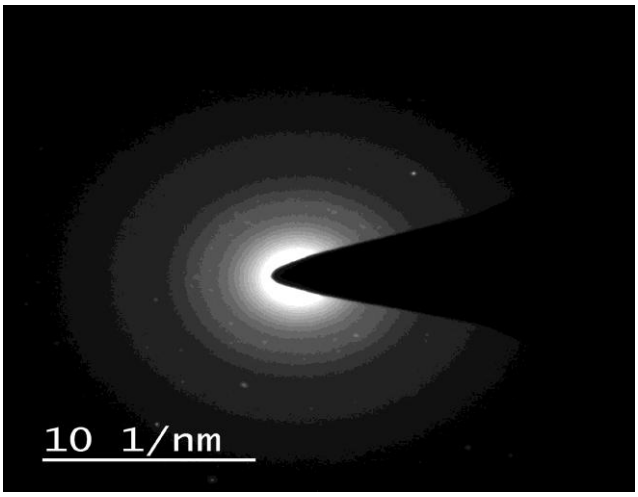

Figure 5.18 Selected area electron diffraction pattern of optimized DSB-PEG-Ch-GNPs

The surface topographic 2D and 3D AFM micrographs of the optimized DSB-PEG-Ch-GNPs are depicted in Figure 5.19 (A) and (B), respectively. The AFM micrographs showed uniform spherical shaped, smooth surfaced DSB-PEG-Ch-GNPs devoid of any visible perforations and agglomerations. The possible reason for this could be the stabilization by PEG and its uniform covering over the surface.

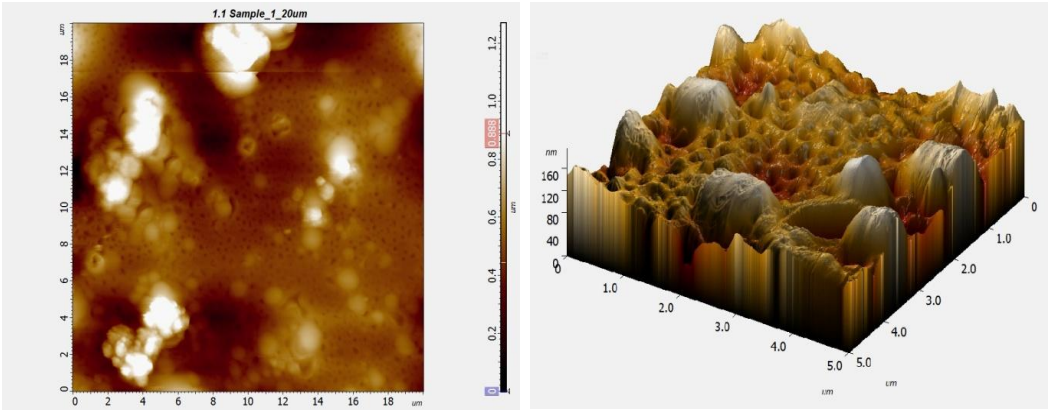

(A) **(B)**

Figure 5.19 2D atomic force microscopy micrograph of optimized DSB-PEG-Ch-GNPs (A) and 3D atomic force microscopy micrograph of optimized DSB-PEG-Ch-GNPs (B)

5.3.5 Stability study

Stability study results of optimized DSB-PEG-Ch-GNPs are shown in Table 5.15. The physical appearance of the optimized DSB-PEG-Ch-GNPs nanoformulation did not show any significant change in accelerated (40 ± 2^0 C / 75 ± 5% RH), room temperature (25 ± 2^0 C) and refrigerated (4 ±1^0 C) storage conditions. As shown in Figure 5.20 (A, B and C) no significant ($p > 0.05$) change in the particle size, % entrapment efficiency and zeta potential was observed for DSB-PEG-Ch-GNPs stored at different conditions of storage over a period of 6 months. Therefore, it was inferred that optimized DSB-PEG-Ch-GNPs could be stored in all the three storage conditions.

Table 5.15 Stability study results of optimized DSB-PEG-Ch-GNPs nanoformulation

Storage condition	Response	Day			
		0	60	120	180
Accelerated condition (40 ± 2^0 C / 75 ± 5% RH)	PS (nm)	24.39±1.82	25.12±1.26	27.63±1.45	30.14±1.18
	ZP (mV)	-13.91±1.21	-12.64±1.18	-11.61±1.07	-10.96±1.12
	EE (%)	72.06±0.86	71.42±0.74	70.74±0.69	69.21±0.72
Room temperature (25 ± 2^0 C)	PS (nm)	24.39±1.82	24.81±1.47	25.79±1.52	27.52±1.36
	ZP (mV)	-13.91±1.21	-12.98±1.26	-11.86±1.09	-11.06±1.15
	EE (%)	72.06±0.86	71.86±0.65	70.98±0.72	69.83±0.81
Refrigerated condition (4 ±1^0 C)	PS (nm)	24.39±1.82	24.63±1.54	25.47±1.23	26.92±1.48
	ZP (mV)	-13.91±1.21	-13.06±1.14	-12.27±1.27	-11.29±1.31
	EE (%)	72.06±0.86	71.98±0.62	71.23±0.81	70.16±0.77

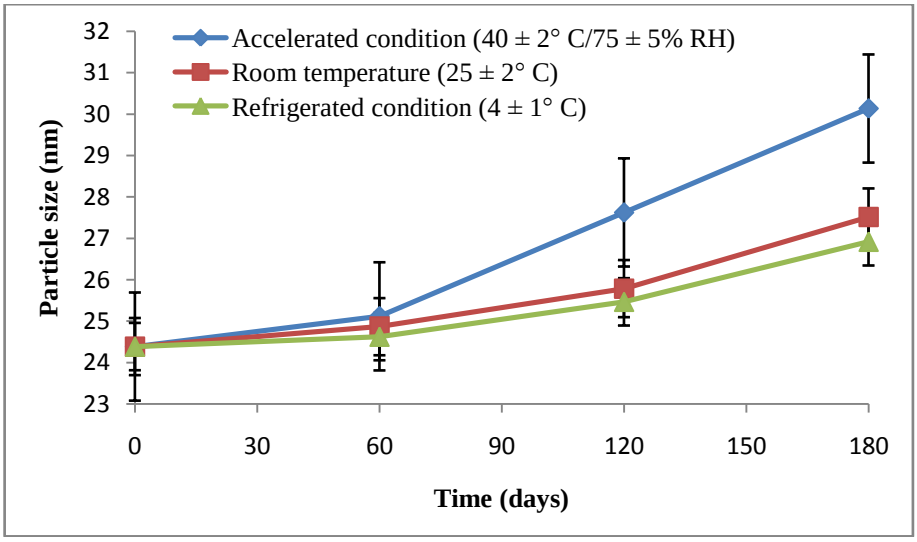

(A)

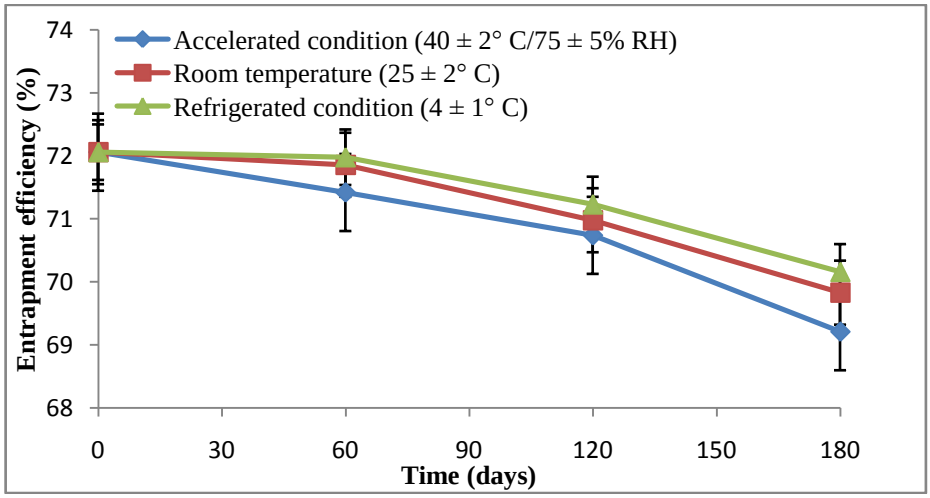

(B)

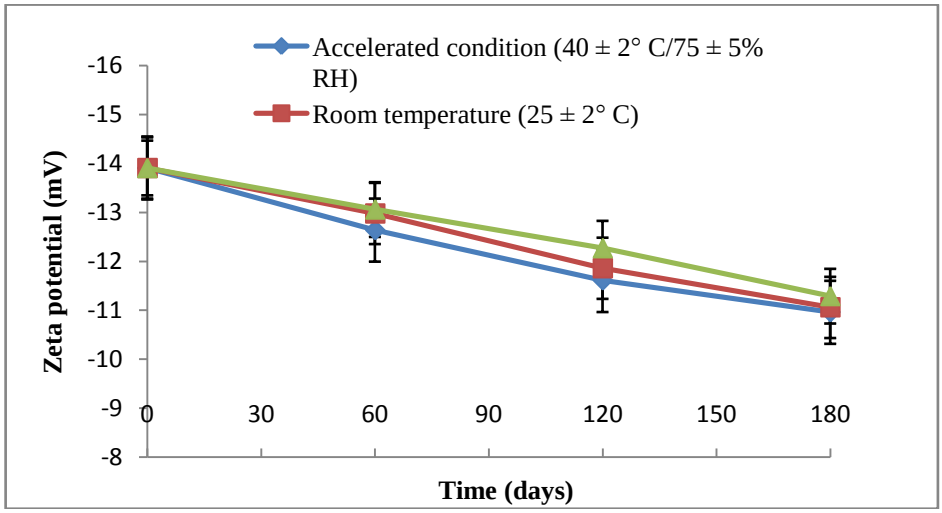

(C)

(vertical bars represents mean ± SD and n = 3)

Figure 5.20 Stability study profiles of particle size (A), % entrapment efficiency (B) and zeta potential (C) of optimized DSB-PEG-Ch-GNPs at different storage conditions and different time intervals

5.3.6 *In vitro* drug release studies

The release pattern of DSB from the optimized DSB-PEG-Ch-GNPs nanoformulation is shown in Figure 5.21. DSB release from the optimized DSB-PEG-Ch-GNPs was observed for 48 hours. Approximately 30% of DSB was released in the first 4 hours and 76% of DSB was released at the end of 48 hours, indicating sustained drug release pattern which is likely due to the strong interaction between DSB/PEG/Ch-GNP conjugates.

Further, the kinetics and drug release mechanism was determined by fitting the *in vitro* drug release profile data of the optimized DSB-PEG-Ch-GNPs nanoformulation to zero-order (R^2 = 0.849), first-order (R^2 = 0.921), Higuchi square root (R^2 = 0.964), Hixon-Crowell cube root (R^2 = 0.900) and Korsmeyer-Peppas (R^2 = 0.978) kinetic models. The release kinetic modeling showed that the drug release kinetics from the optimized DSB-PEG-Ch-GNPs nanoformulation followed Korsmeyer-Peppas model (highest R^2 value).

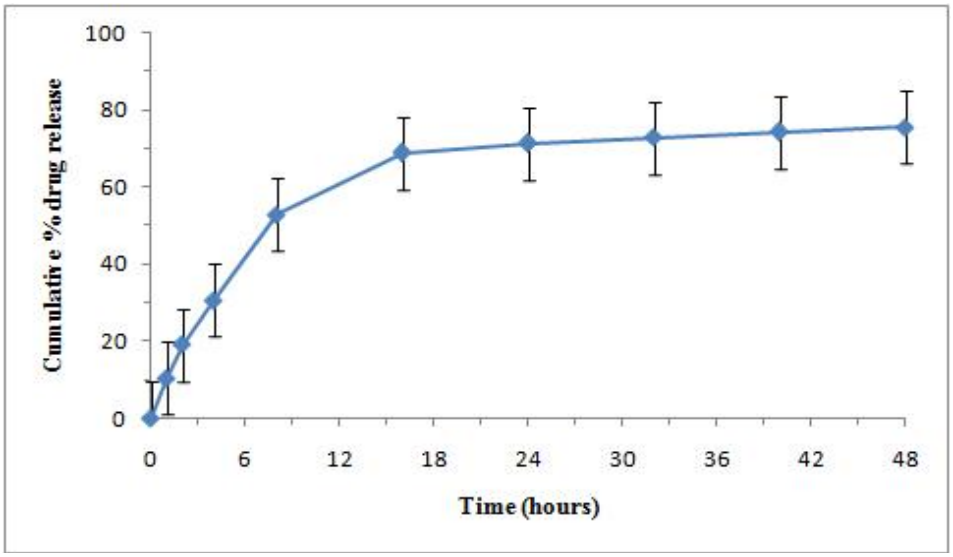

(vertical bars represents mean ± SD and n = 3)

Figure 5.21 *In vitro* drug release profile of the optimized DSB-PEG-Ch-GNPs nanoformulation in pH 7.4 phosphate buffer

5.4 Preparation of DSB loaded PLGA stabilized chitosan capped GNPs (DSB-PLGA-Ch-GNPs)

The synthesized Ch-GNPs were visually observed for the appearance of any color change in the dispersion. A clear deep ruby red color was formed within 1 hour, as a result of bioreduction by chitosan which indicated the green synthesis of Ch-GNPs and the dispersion was examined by UV-Visible spectrophotometry. The dispersion was scanned in the range of 300-800 nm wavelength. In the UV–Vis absorption spectrum, a peak maximum at 525 nm was recorded, which is attributed to the SPR band of GNPs. After the successful synthesis of Ch-GNPs, subsequent stabilization and loading of DSB were done.

5.4.1 Risk identification and risk assessment screening

The potential risk factors that may influence the responses were identified by QbD approach. The cause-effect relationship was systematically explored by a qualitative graphical tool i.e., Ishikawa fish bone [Mukharya et al., 2013]. On the basis of the prior experimentation, eight factors (X_1-X_8) were prioritized and screened further.

As the number of independent variables was more, risk assessment screening was performed to reduce the sets of independent variables to those that have the most influence on the dependent variables. Screening was done by the DOE approach of eight factors, two level PBD using Minitab 17 software. The independent variables used in the experimentation were A - PLGA concentration, B - stirring speed, C - stirring time, D - sonication time, E - sonication frequency, F - temperature, G - centrifugation time, and H - centrifugation speed. All the unique properties of the GNPs are influenced by its particle size. Through preliminary screening by PBD, PLGA concentration, stirring time and sonication time were identified as the most significant variables within the range of 0.01-0.10 % w/w, 4-8 hours, 10-30 mins, respectively. The rate and extent

of drug uptake in the cellular microenvironment is the main aspect that decides the therapeutic efficacy of the DSB-PLGA-Ch-GNPs. In order to attain this, nanoparticles with appropriate % entrapment efficiency and good release from the nanocarrier ensuring the sustained concentration of DSB at the site of uptake is desirable. The long term physical stability of the prepared nanoformulation is necessary, and zeta potential is a key indicator for ensuring it. Hence, particle size, % entrapment efficiency and zeta potential selected as responses. A total of 12 experimental runs were generated with particle size, % entrapment efficiency and zeta potential (Table 5.16). PLGA concentration, ST, and SoT were identified as significant variables that influenced the responses through preliminary screening by PBD. ANOVA was employed to evaluate the significance of PBD and statistically significant coefficients for each factor. Subsequently, Pareto charts were generated in order to screen out the main significant factors influencing the responses (Figure 5.22).

Table 5.16 Composition of nanoformulation showing the levels of various factors and the results of observed mean values of various responses by Plackett-Burman Design

Run	X_1	X_2	X_3	X_4	X_5	X_6	X_7	X_8	Y_1*	Y_2*	Y_3*
1	+	-	+	-	-	-	+	+	30.29±0.46	66.94±0.54	-10.56±0.08
2	+	-	+	+	-	+	-	-	20.94±0.58	79.84±0.42	-13.04±0.08
3	-	-	-	+	+	+	-	+	22.47±0.42	43.10±0.28	-14.22±0.10
4	-	-	-	-	-	-	-	-	32.98±0.32	53.66±0.08	-13.06±0.12
5	-	+	+	+	-	+	+	-	12.18±0.52	71.58±0.64	-18.14±0.02
6	-	-	+	+	+	-	+	+	14.25±0.84	61.24±0.46	-13.84±0.10
7	+	+	-	+	+	-	+	-	24.02±0.18	73.92±0.56	-12.08±0.06
8	+	+	+	-	+	+	-	+	27.14±0.76	57.08±0.92	-12.67±0.06
9	-	+	-	-	-	+	+	+	28.76±0.81	44.16±0.24	-16.94±0.14
10	+	+	-	+	-	-	-	+	25.34±0.23	77.14±0.85	-10.96±0.10
11	+	-	-	-	+	+	+	-	31.93±0.38	61.22±0.61	-12.42±0.06
12	-	+	+	-	+	-	-	-	16.08±0.24	42.24±0.35	-17.24±0.14

(Note: + high level, - low level; * Mean ± SD, n = 3)

[X_1 - PLGA concentration; X_2 - stirring speed; X_3 - stirring time; X_4 - sonication time; X_5 - sonication frequency; X_6 - temperature; X_7 - centrifugation time; X_8 - centrifugation speed; Y_1 - particle size; Y_2 - % entrapment efficiency and Y_3 - zeta potential].

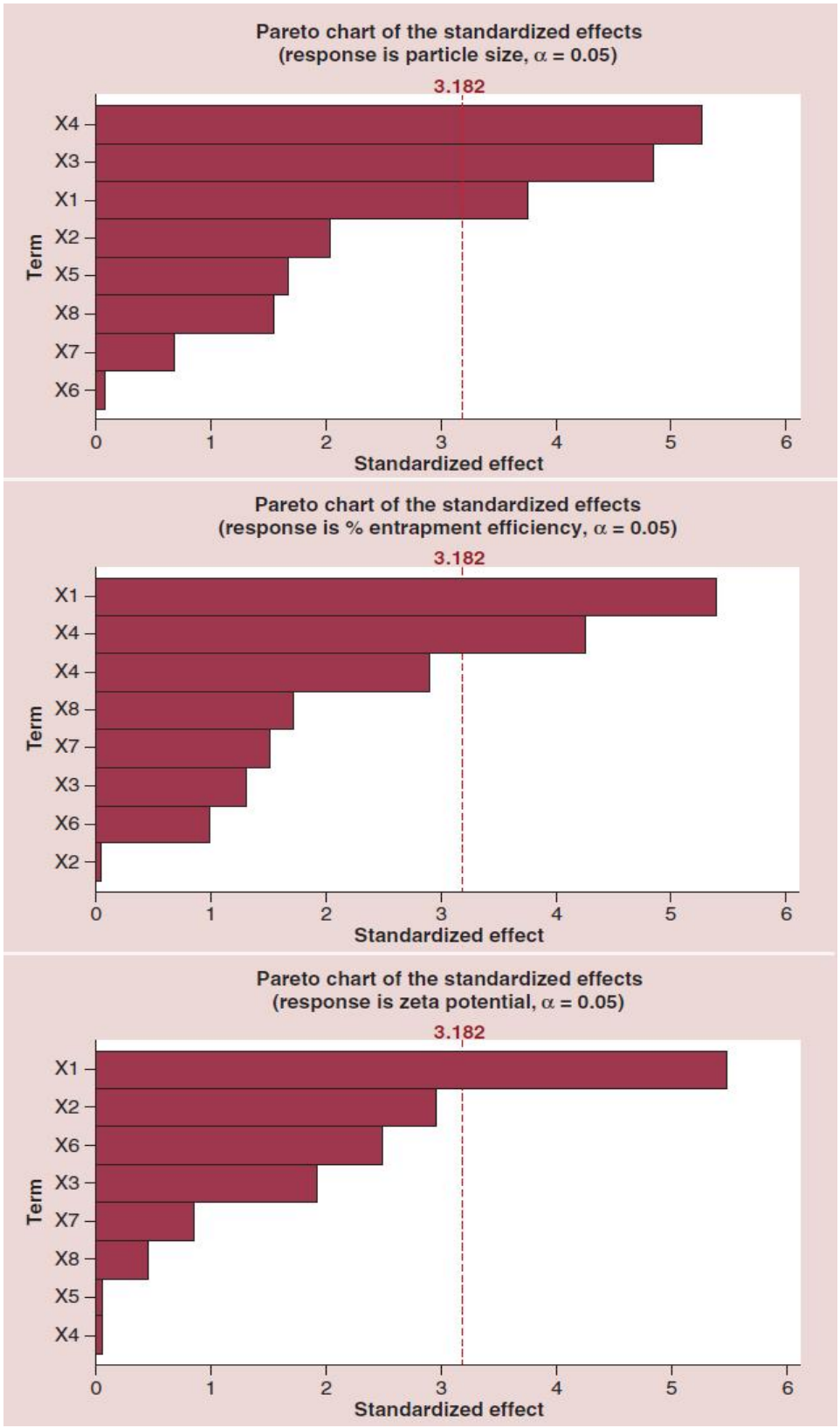

X_1-PLGA concentration; X_2-Stirring speed; X_3-Stirring time; X_4-Sonication time; X_5-Sonication frequency; X_6-Temperature; X_7-Centrifugation time and X_8-Centrifugation speed

Figure 5.22 Pareto charts showing the influence of significant factors on responses (particle size, % entrapment efficiency and zeta potential) of DSB-GNPs

5.4.2 2^3 full factorial design

The formulation design was carried out using response surface method by 3 factor, 2 level, and 3 response full factorial design and systematically explored the main, quadratic and interaction effects of each individual factor on the responses (Table 5.17). A total of 8 randomized experimental runs were generated, and the experiments were performed accordingly. Experimental runs were conducted, and the results of PS, % EE and ZP are shown in Table 5.18. The regression equations were generated for each response and a '+' sign in front specifies synergistic effect while '-' sign specifies the antagonistic effect of the independent variables [Pund et al., 2014]. 3D response surface plots were used to enumerate the interaction and correlation between the factors and the measured responses. ANOVA was used to carry out the data analysis and estimation of the quantitative effect of the factors.

Table 5.17 List of the three factors, their levels in the 2^3 full factorial design along with the responses

Independent variables (Factors)	**Name**	**Unit**	**Min.**	**Max.**
X_1	PLGA concentration	% w/w	0.01	0.10
X_2	Stirring time	hours	4	8
X_3	Sonication time	mins	10	30
Dependent variables (Responses)	**Name**	**Unit**	**Constraint**	
Y_1	Particle size	nm	Minimize	
Y_2	% Entrapment efficiency	%	Maximize	
Y_3	Zeta potential	mV	Minimize	

Table 5.18 2^3 full factorial design matrix and results of observed mean values of various responses

Run	X_1	X_2	X_3	Y_1*	Y_2*	Y_3*
FD-1	0.10	8	10	29.48±0.94	76.84±0.27	-12.97±1.04
FD-2	0.01	4	30	26.36±1.24	65.87±0.92	-16.37±1.08
FD-3	0.10	4	10	31.84±1.04	73.54±0.28	-10.37±1.08
FD-4	0.01	8	30	24.18±1.52	69.28±0.94	-18.54±1.06
FD-5	0.10	8	30	28.96±1.28	78.62±0.48	-13.28±1.02
FD-6	0.10	4	30	30.82±1.32	74.31±0.64	-11.08±1.12
FD-7	0.01	4	10	26.98±1.18	62.98±0.76	-15.96±1.04
FD-8	0.01	8	10	25.22±1.62	68.48±0.94	-17.26±1.06

(* Mean ± SD, n = 3)
[X_1 - PLGA concentration; X_2 - stirring time; X_3 - sonication time; Y_1 - particle size; Y_2 - % entrapment efficiency and Y_3 - zeta potential].

5.4.2.1 Influence of independent variables on PS

PS is a significant response which influences the drug payload, biodistribution, ability to target and toxicity [Singh and Lillard, 2009] The mean PS of the optimized DSB-PLGA-Ch-GNPs nanoformulation developed according to the 2^3 FFD was in the range of 24.18 ± 1.52 nm to 31.84 ± 1.04 nm. The polynomial equation generated by the FFD showing the effect of factors on PS is as follows:

$Y_1 = 28.16 + 68.00\ A - 0.358\ B - 0.0026\ C - 2.944\ AB - 0.733\ AC - 0.0065\ BC + 0.127\ ABC$

It was found that there was a significant effect of PC on the PS. A synergistic effect was observed between PC and PS, such that an increase in PC resulted in an increase in PS. The interaction and correlation between the factors and PS were further explained by 3D response surface plots, and its corresponding graphs are shown in Figure 5.23 (A and B). Although, PC seems to be the most significant factor affecting the PS of the optimized DSB-PLGA-Ch-GNPs nanoformulation; however, the final size

was influenced by the ST as well as the SoT. More the ST and SoT more will be the mechanical and hydraulic shear which can effectively reduce the PS. The quadratic model's ANOVA analysis generated for PS indicated an excellent fit between predicted values and experimental results, there was no lack of fit (>0.05), and thus the model can be used to plot the optimized design space.

5.4.2.2 Influence of independent variables on % EE

In order to reduce the dose, the nanoparticles should have high % EE. DSB is a high dose drug and to reduce its dose related adverse effects and to improve its efficacy, lowering of the dose is necessary. The % EE of the optimized DSB-PLGA-Ch-GNPs nanoformulation developed according to the 2^3 FFD was in the range of 62.98 ± 0.76 % to 78.62 ± 0.48 %. The impact of PC on the % EE was more significant than the effects of the ST and SoT. The polynomial equation generated by the FFD showing the effect of factors on % EE is as follows:

$Y_2 = 53.28 + 170.8\ A + 1.740\ B + 0.278\ C - 10.42\ AB - 2.90\ AC - 0.030\ BC + 0.430\ ABC$

The % EE was decreased at a high ST which was mainly due to the diffusion of the DSB out of the nanoparticles during the size reduction stage. 3D response surface plot of the optimized DSB-PLGA-Ch-GNPs nanoformulation is shown in Figure 5.23 (C). The quadratic model's ANOVA analysis generated for % EE indicated an excellent fit between predicted values and experimental results, there was no lack of fit (>0.05), and thus the model can be used to plot the optimized design space.

5.4.2.3 Influence of independent variables on ZP

The ZP of the optimized DSB-PLGA-Ch-GNPs nanoformulation developed according to the 2^3 FFD was in the range of -10.37 ± 1.08 mV to -18.54 ± 1.06 mV. The

polynomial equation generated by the FFD showing the effect of factors on ZP is as follows:

$Y_3 = 15.74 - 85.28\,A + 0.162\,B - 0.0317\,C + 5.375\,AB + 0.872\,AC + 0.0126\,BC - 0.176\,ABC$

The interaction and correlation between the factors and ZP were further explained by the 3D response surface plot, and its corresponding graph is shown in Figure 5.23 (D). The quadratic model's ANOVA analysis generated for ZP indicated an excellent fit between predicted values and experimental results, there was no lack of fit (>0.05), and thus the model can be used to plot the optimized design space.

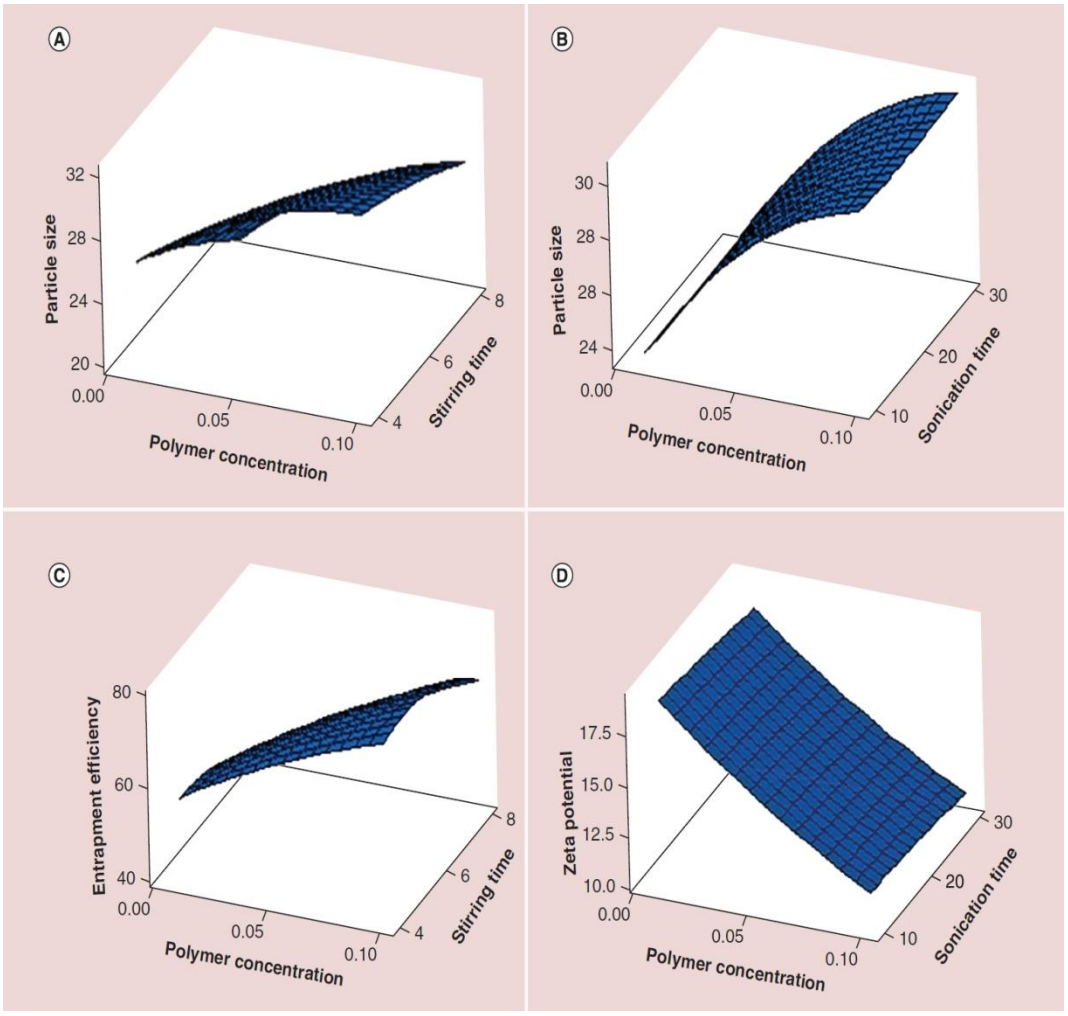

Figure 5.23 The 3D response surface plots showing the effect of PLGA concentration, stirring time and sonication time on particle size (A & B), % entrapment efficiency (C) and zeta potential (D)

In order to achieve nanoparticles of highest % EE with required PS and ZP, response optimization was performed and the optimal conditions of PC, ST and SoT were found to be 0.098 % w/w, 8 hours and 30 minutes, respectively. Particle size, zeta potential and % entrapment efficiency were predicted as 26.94 nm, -15.46 mV and 80.72 %, respectively (Table 5.19).

Table 5.19 The predicted and experimental values for all the responses observed for optimized DSB-PLGA-Ch-GNPs nanoformulation

Factors for response optimization		
X_1 – PLGA concentration (% w/w)	0.098	
X_2 – Stirring time (hours)	8	
X_3 – Sonication time (minutes)	30	
Optimized results		
Responses	**Predicted value**	**Experimental value***
Y_1 – Particle size (nm)	28.88	26.94 ± 1.14
Y_2 – % Entrapment efficiency (%)	78.47	80.72 ± 0.58
Y_3 – Zeta potential (mV)	-13.36	-15.46 ± 1.06

(* Mean ± SD, n = 3)

5.4.3 PS, % EE and ZP

The mean particle size of the optimized nanoformulation of DSB-PLGA-Ch-GNPs was found to be 26.94 ± 1.14 nm as compared to the DSB-PEG-Ch-GNPs (30.90 ± 1.14 nm) and DSB-PVP-Ch-GNPs (24.39 ± 1.82 nm). The nanoformulations developed were having a particle size of 20 to 40 nm, which plays a pivotal role in the targeted drug delivery (Figure 5.24 (A)). When the concentration of the polymer increased, the nanoparticles with larger particle size were obtained. The mean % entrapment efficiency of the optimized nanoformulation of DSB-PLGA-Ch-GNPs was found to be 80.72 ± 0.58 % as compared to the DSB-PEG-Ch-GNPs (72.06 ± 0.86 %) and DSB-PVP-Ch-GNPs (61.02 ± 0.39 %). High % entrapment efficiency is desirable as it carries high drug payload and influences the rate and extent of drug uptake in the cellular

microenvironment, the therapeutic efficacy of the nanoformulation and ultimately the sustained release of the drug at the site of uptake. The mean zeta potential of the optimized nanoformulation of DSB-PLGA-Ch-GNPs was found to be -15.46 ± 1.06 mV as compared to the DSB-PEG-Ch-GNPs (-13.91 ± 1.21 mV) and DSB-PVP-Ch-GNPs (-14.08 ± 1.02 %). Zeta potential of all the prepared nanoformulations were within the acceptable limits and it is a key indicator for ensuring long term physical stability of the prepared nanoformulations (Figure 5.24 (B)).

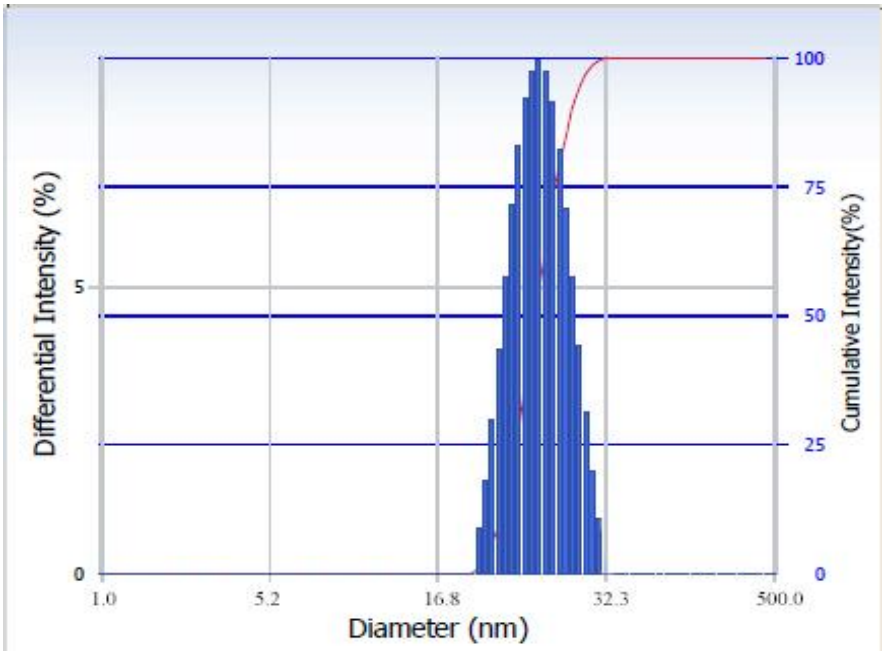

(A)

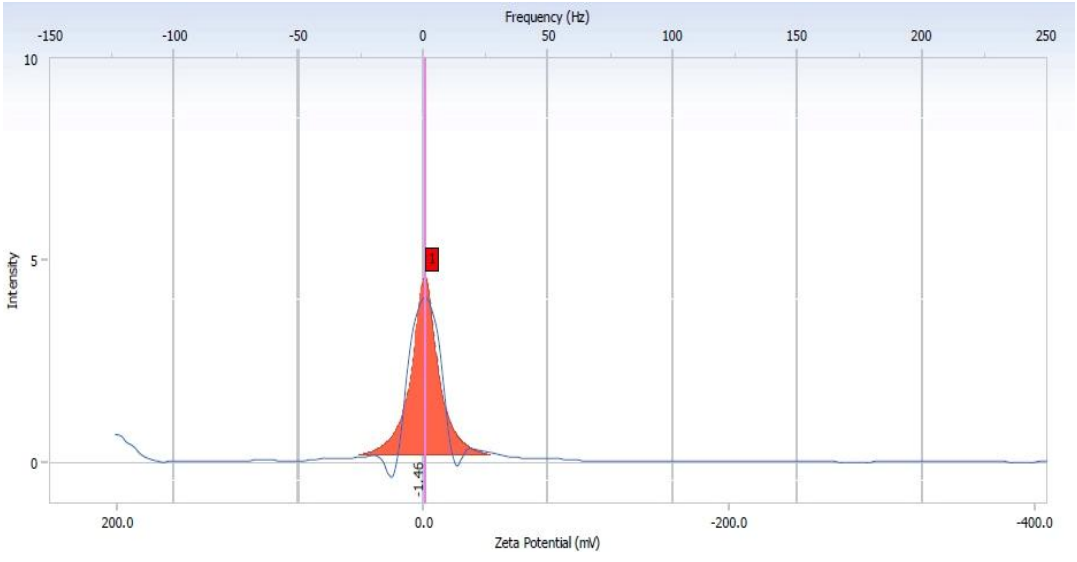

(B)

Figure 5.24 Graphs of (A) intensity distribution (particle size) and (B) mobility distribution (zeta potential) of optimized DSB-PLGA-Ch-GNPs nanoformulation

5.4.4 Solid state characterization of optimized nanoformulation

The physicochemical characteristics, compatibility and effectiveness of the drug and the excipients used in the development of the formulation were determined by FTIR and XRD. The physical and chemical interaction between the drug-excipients used in the development of the nanoformulation affects the overall characteristics of the final dosage form.

FTIR overlay spectrum of optimized DSB-PLGA-Ch-GNPs nanoformulation along with DSB, PLGA, Ch, and GNPs is shown in Figure 5.25. FTIR spectrum of DSB revealed characteristic bands at 1620.26 cm^{-1} (C═O stretching), 2949.26 cm^{-1} (C-H stretching), 3026.41 cm^{-1} (-C-H aromatic ring), 3201.94 cm^{-1} (O-H stretching), and 3417.98 cm^{-1} (N-H stretching). For chitosan spectrum, the bands were observed at 1031.95 cm^{-1}(C-O stretching), 1321.28 cm^{-1} (C-H), 1564.32 cm^{-1} (N-H), 1654.98 cm^{-1} (–NH2), and 3385.18 cm^{-1} (-N-H). In case of PLGA the bands appeared at 750.33 cm^{-1} (C–H bending), 1047.38 cm^{-1} (-C-CH_3), 1186.26 cm^{-1} (-C-O stretching), 1384.94 cm^{-1} (O–H bending), 1456.30 cm^{-1} (C-H stretching), and 1755.28 cm^{-1} (-C=O stretching).

XRD overlay spectrum of optimized DSB-PLGA-Ch-GNPs nanoformulation along with DSB, PLGA, Ch, and GNPs is shown in Figure 5.26. XRD spectrum of DSB exhibited its crystalline nature with well resolved and relatively intense peaks at 2θ angles of 21.11°, 21.85°, 22.11°, 23.13°, 24.42°, 25.32°, 27.81°. The diffraction patterns of the PLGA, Ch, and Ch-GNPs showed various small diffuse peaks with the broad halo. The XRD spectrum of the DSB-PLGA-Ch-GNPs exhibited broad diffuse peaks resulting in the decrease in the crystalline nature of the DSB, suggesting that DSB had been converted into amorphous nature.

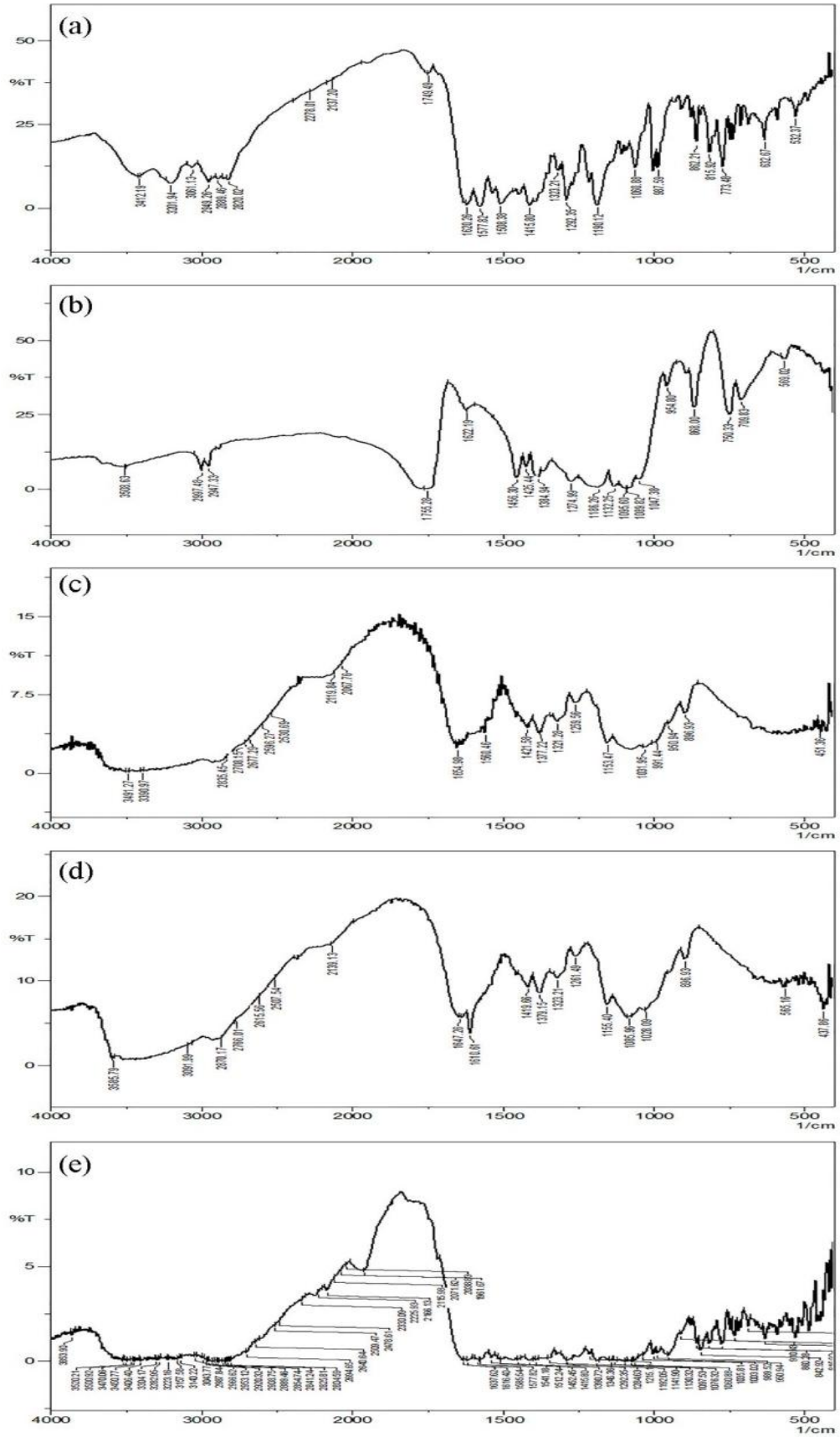

(a) DSB; (b) PLGA; (c) Ch; (d) GNPs and (e) Optimized nanoformulation.

Figure 5.25 FTIR overlay spectrum of DSB-PLGA-Ch-GNPs

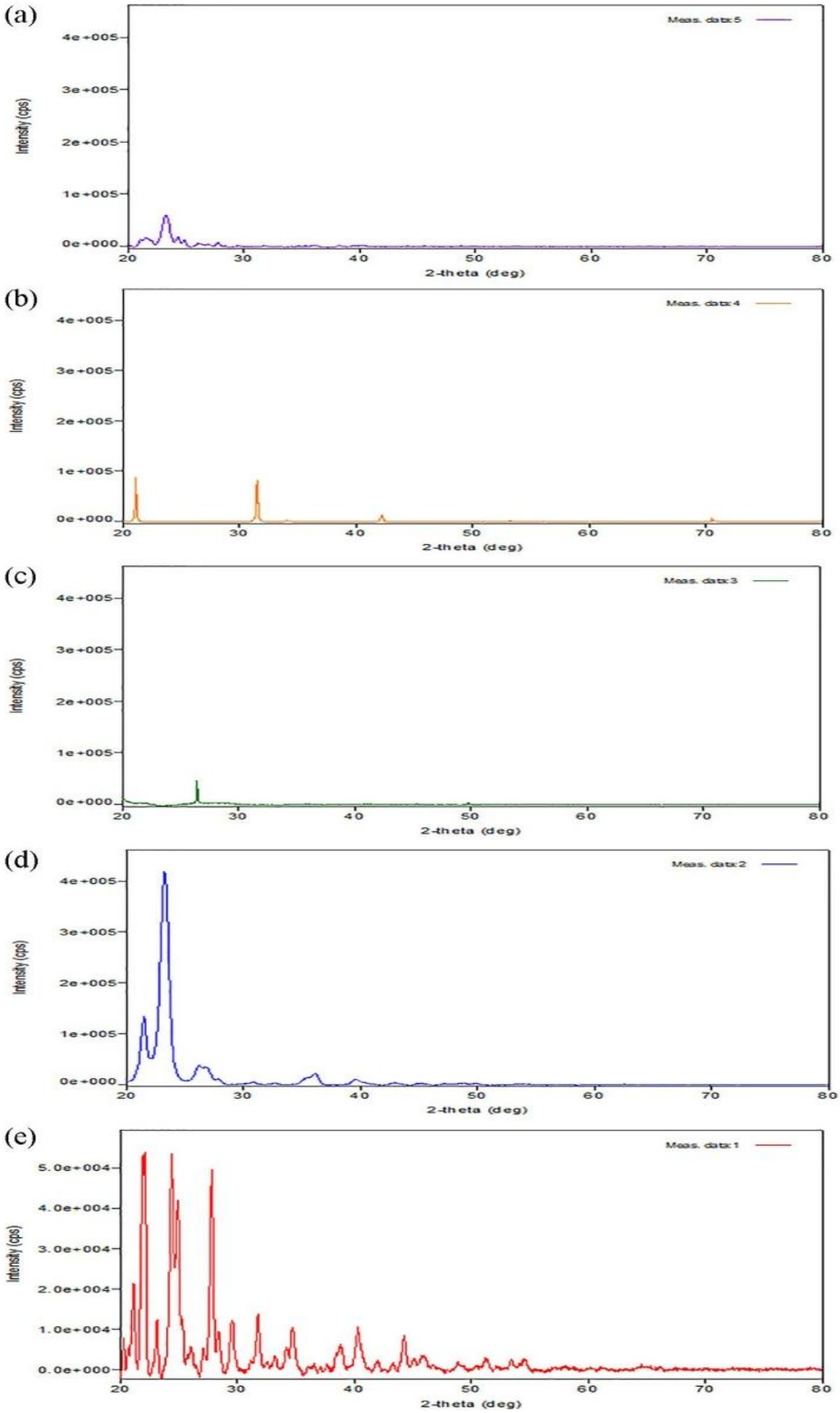

(a) DSB; (b) PLGA; (c) Ch; (d) GNPs and (e) Optimized nanoformulation.

Figure 5.26 XRD overlay spectrum of DSB-PLGA-Ch-GNPs

5.4.5 Physicochemical and morphological characterization

As the mean PS were in the size of around 27 nm, the HR-SEM micrographs (Figure 5.27 (A and B)) resolution was limited, and no clear differences in morphology were observed, so TEM was employed. Sharp and clear peaks of gold (Au) in the EDS spectrum (Figure 5.27 (C)) confirmed the successful reduction of the gold chloride hydrate. In addition, small peaks of carbon (C) and other atoms were originated due to the molecules that were used in the preparation of DSB-GNPs and Copper (Cu) due to use of the copper grid over which the optimized DSB-PLGA-Ch-GNPs nanoformulation was placed. Further, the spatial distribution of gold in the optimized DSB-PLGA-Ch-GNPs nanoformulation is shown by colour mapping report in Figure 5.27 (D).

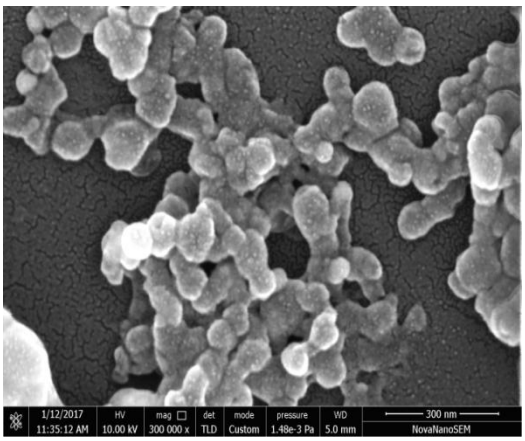

(A)

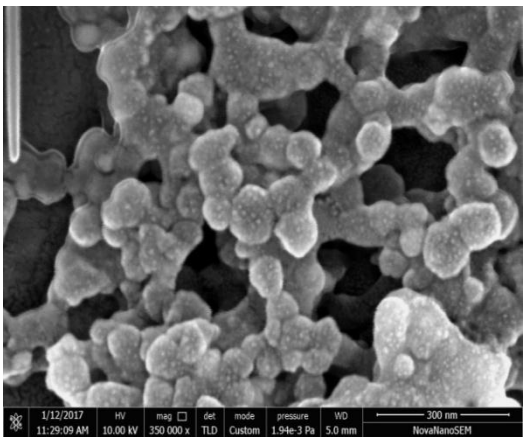

(B)

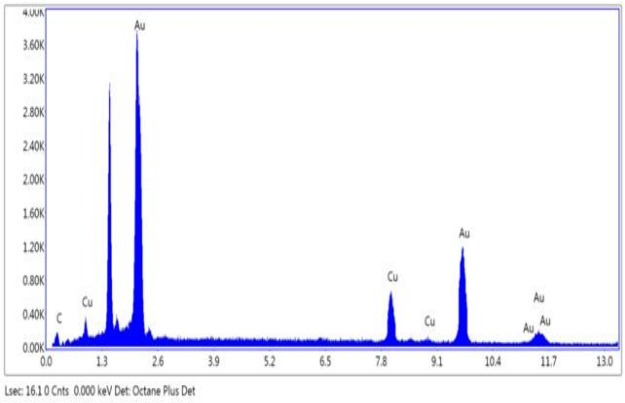

(C)

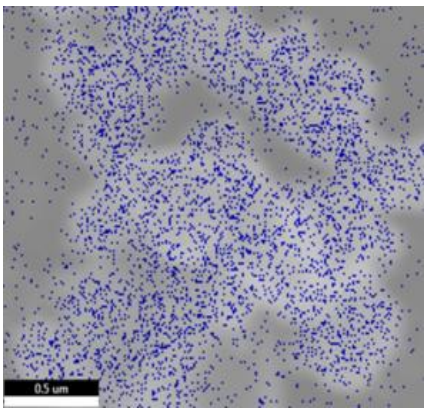

(D)

Figure 5.27 HR-SEM micrographs (A & B), EDS spectrum (C), and Colour mapping report of the spatial distribution of gold in the optimized DSB-PLGA-Ch-GNPs nanoformulation (D)

To determine the surface morphology of the optimized nanoformulation of DSB-PLGA-Ch-GNPs, TEM analysis was performed. TEM micrographs (Figure 5.28 (A, B)) revealed a clear core-shell structure. The GNPs were appeared to be smooth, spherical and without any ruptures at different magnifications. The core (gold) was dark, and the shell (envelop) was lighter because of the difference in their electron densities. Further, the SAED pattern of the optimized DSB-PLGA-Ch-GNPs nanoformulation showed bright circular spots and characteristic diffraction ring patters (Figure 5.28 (C)).

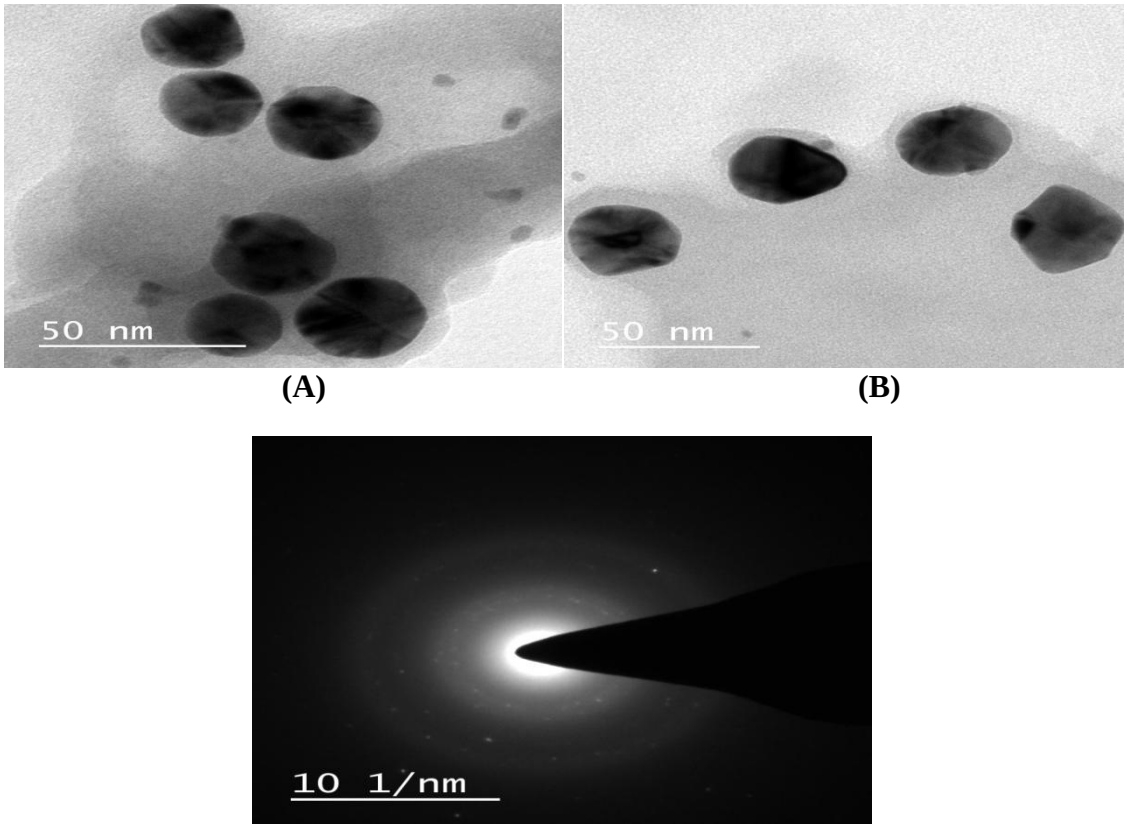

(A) **(B)**

(C)

Figure 5.28 TEM micrographs (A, B) and SAED pattern (C) of the optimized DSB-PLGA-Ch-GNPs nanoformulation

2D and 3D surface topographic AFM micrographs of the optimized DSB-PLGA-Ch-GNPs nanoformulation showed uniform, smooth surfaced spherical

nanoparticles without any perforations and agglomerates (Figure 5.29). This was achieved mainly due to the stabilization and uniform covering by the PLGA over the DSB-GNP's surface.

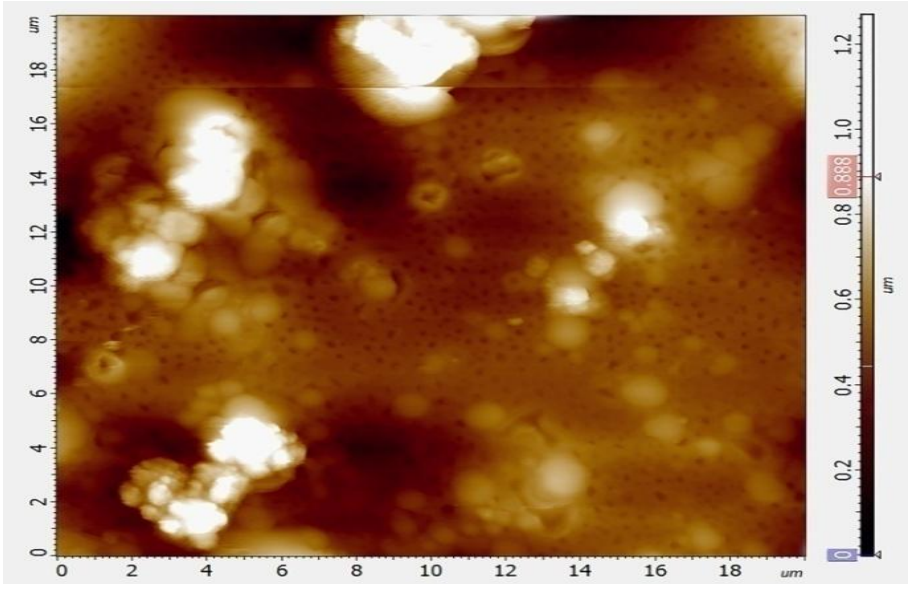

(A)

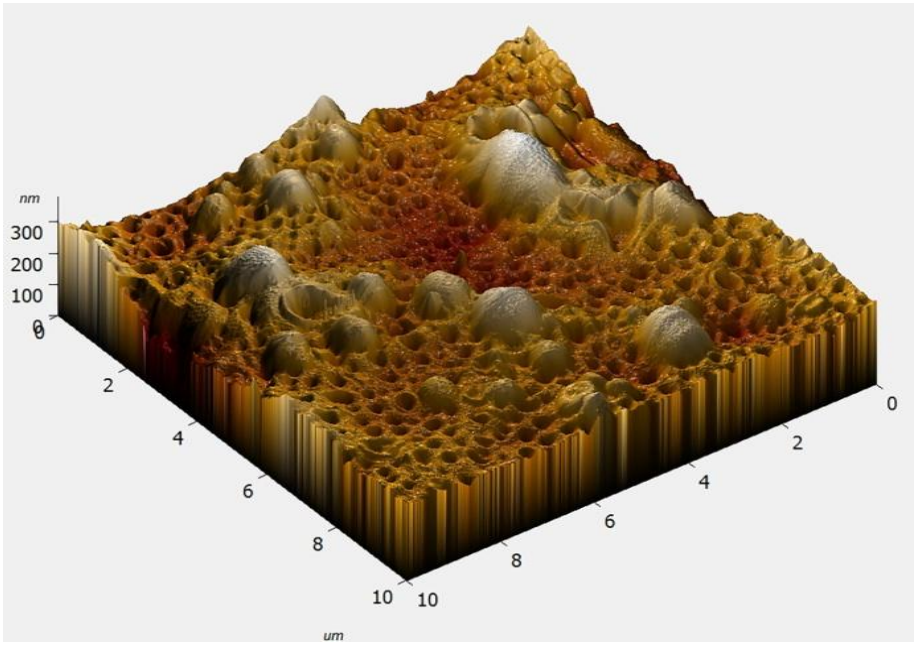

(B)

Figure 5.29 2D AFM micrograph (A) and 3D AFM micrograph (B) of the optimized DSB-PLGA-Ch-GNPs nanoformulation

5.4.6 Stability study

Stability study of the optimized DSB-PLGA-Ch-GNPs nanoformulation was performed as per ICH guidelines at 40 °C ± 2 °C / 75% RH ± 5% RH (accelerated), 25 °C ± 2 °C (room temperature) and 4 °C ± 1 °C (refrigerated) conditions for a period of 6 months and the results are presented in Table 5.20 and Figure 5.30. No significant change in the physical appearance as well as in the PS, % EE and ZP of the optimized DSB-PLGA-Ch-GNPs nanoformulation was observed at the accelerated condition, room temperature and refrigerated condition over a period of 6 months.

Table 5.20 Stability study results of optimized DSB-PLGA-Ch-GNPs nanoformulation

Storage condition	Response	Day			
		0	60	120	180
Accelerated condition (40 ± 2^0 C / 75 ± 5% RH)	PS (nm)	26.94±1.14	27.35±1.21	28.34±1.19	30.12±1.05
	ZP (mV)	-15.45±0.58	-14.19±0.84	-13.18±0.62	-12.54±0.68
	EE (%)	80.72±1.06	80.12±1.18	79.46±1.24	78.36±1.12
Room temperature (25 ± 2^0 C)	PS (nm)	26.94±1.14	27.14±1.05	27.66±1.42	28.72±1.25
	ZP (mV)	-15.45±0.58	-14.44±0.67	-13.42±0.74	-12.61±0.45
	EE (%)	80.72±1.06	80.34±1.20	79.95±1.18	79.08±1.27
Refrigerated condition (4 ± 1^0 C)	PS (nm)	26.94±1.14	27.02±1.26	27.32±1.12	27.94±1.35
	ZP (mV)	-15.45±0.58	-14.61±0.75	-13.84±0.64	-12.78±0.52
	EE (%)	80.72±1.06	80.56±1.22	80.28±1.13	79.56±1.25

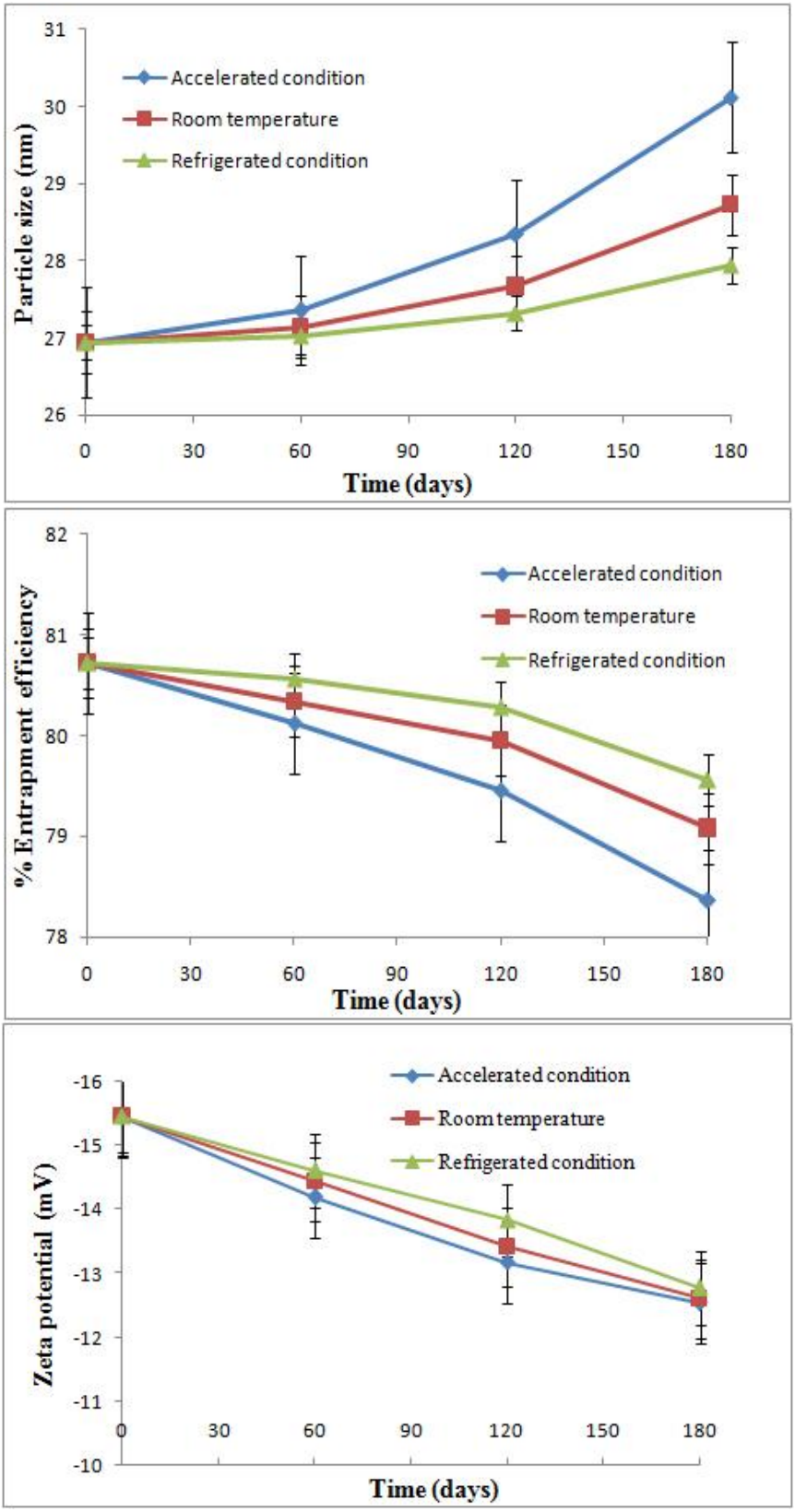

(vertical bars represents mean ± SD and n = 3)

Figure 5.30 Stability study profiles of optimized DSB-PLGA-Ch-GNPs nanoformulation for particle size, % entrapment efficiency and zeta potential at different storage conditions and different time intervals

5.4.7 *In vitro* drug release study

The *in vitro* DSB release profile from the optimized DSB-PLGA-Ch-GNPs nanoformulation showed 32 % of the DSB release in the first 4 hours, and 79 % of the DSB release at the end of 48 hours (Figure 5.31).

Further, to determine the mechanism of DSB release, the *in vitro* DSB release data of the optimized DSB-PLGA-Ch-GNPs nanoformulation was fitted to five different mathematical models for drug release kinetics. The drug release followed Korsmeyer-Peppas (R^2 = 0.978) kinetics and exhibited sustained drug release.

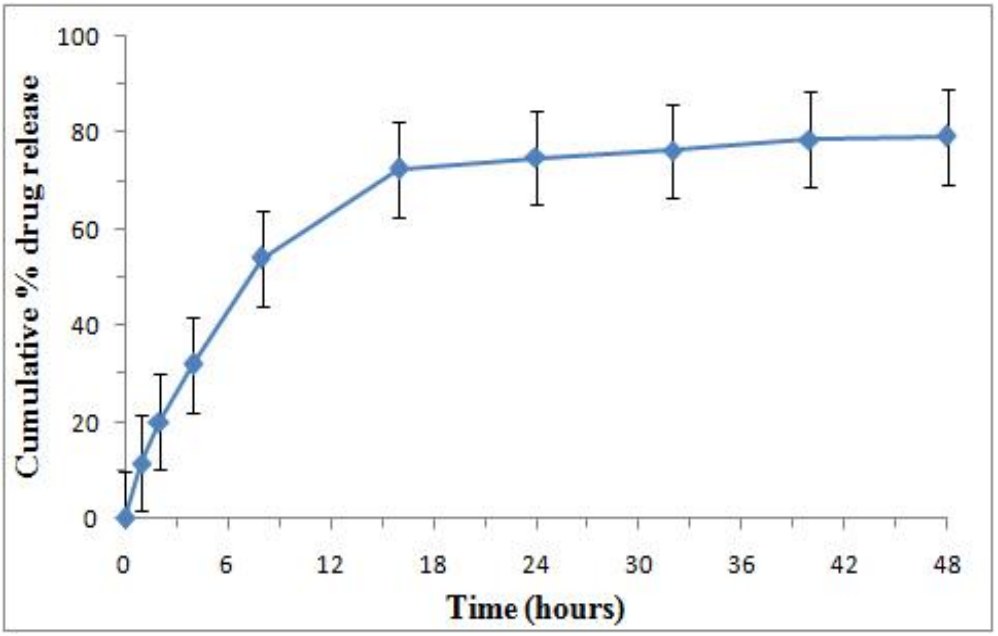

(vertical bars represents mean ± SD and n = 3)

Figure 5.31 *In vitro* drug release profile of the optimized DSB-PLGA-Ch-GNPs nanoformulation in pH 7.4 phosphate buffer

The comparative cumulative percentage of drug release vs. time profiles of all the three nanoformulations are shown in Figure 5.32. From the drug release profiles, it was confirmed that initially drug released was comparatively faster and then followed a slow release pattern for all the three batches of prepared nanoformulations. The optimized DSB-PLGA-Ch-GNPs nanoformulation exhibited a maximum sustaining effect on the drug release followed by DSB-PEG-Ch-GNPs and DSB-PVP-Ch-GNPs.

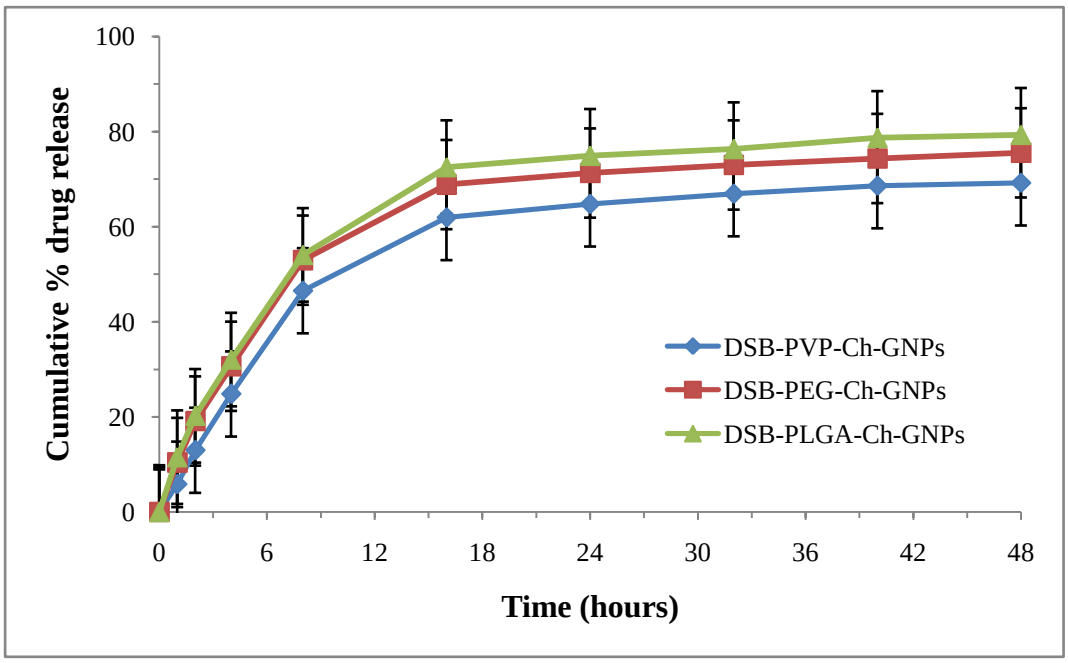

(vertical bars represents mean ± SD and n = 3)

Figure 5.32 Comparative *in vitro* drug release profiles of all the three nanoformulations

5.4.8 *In vitro* hemocompatibility study

For any dosage form that is intended to administer intravenously, the evaluation of hemolysis is mandatory. An *in vitro* hemocompatibility study was performed for the optimized nanoformulation in order to test the hemolytic potential. The blood sample collected from the rat through retro orbital plexus was centrifuged and to the separated erythrocyte sample equal volume of PBS solution was added, and again centrifuged for 10 more minutes at 4000 rpm. To the erythrocyte suspension, different concentrations of optimized nanoformulation (DSB-PLGA-Ch-GNPs) (10-200 µg/ml) were added and incubated at 37 ^{0}C for 45 mins. The resulting sample was stained with hematoxylin and eosin (H & E) stain and visualized the resulting blood smear through Dewinter optical microscope. The results showed that there was no sign of hemolysis when different concentrations of optimized nanoformulation were added to the erythrocyte suspension. This indicates that the optimized DSB-PLGA-Ch-GNPs nanoformulation exhibit no

hemolysis after intravenous administration and makes a safe, compatible and suitable candidate for the application.

5.4.9 Cellular uptake study by confocal fluorescence microscopy

The most important and crucial feature that plays a key role in the success of targeted drug delivery systems is the internalization of the developed nanoparticles. The success of this feature can demonstrate their therapeutic efficacy through intracellular release. K562 human myeloid leukaemia cell lines treated with the drug and optimized nanoformulation (DSB-PLGA-Ch-GNPs) were used for the cellular uptake study. K562 cells after incubation with DSB and optimized nanoformulation are shown in Figure 5.33. The fluorescence of the GNPs was higher and showed more intensity than that of the DSB. The pixel intensities obtained from the confocal fluorescence microscopy was used to generate the fluorescence intensity curves (Figure 5.34). It was observed that the intracellular fluorescence of the optimized nanoformulation of DSB-PLGA-Ch-GNPs was increased with the increase of the incubation time from 4 to 6 hours. It was also observed that DSB loaded GNPs showed approximately 10 to 20 fold much higher intracellular fluorescence intensities than that of DSB (pure drug) alone for the most part of the K562 cell line. These results indicated that the DSB from the DSB loaded GNPs could be readily permeated and accumulated into the leukaemia cancer cells through GNPs. Thus, it was evident that the DSB loaded GNPs could assist the drug targeting and cellular uptake of DSB into leukaemia cancer cells and act as an efficient nanocarrier system to facilitate the relevant drug delivery.

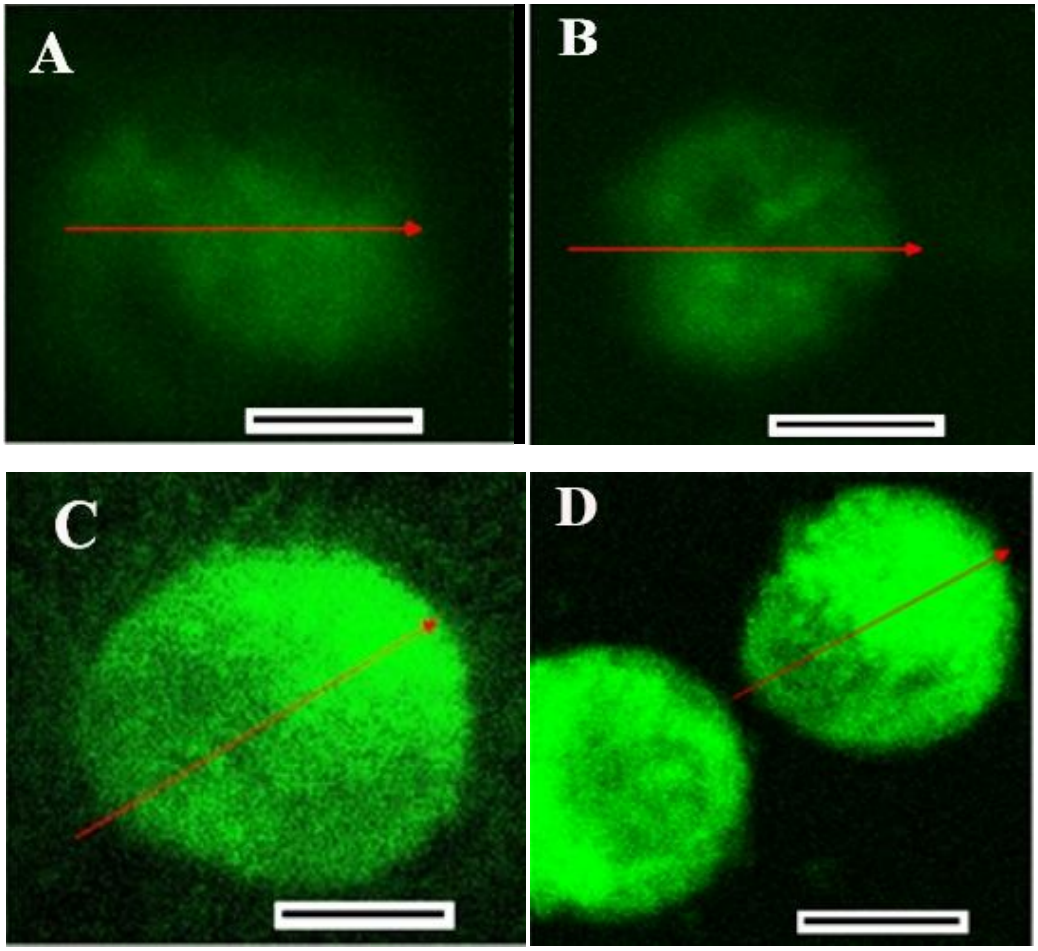

Scale bar- 5 μm; arrows - sampling direction

Note: A, C were images of treated K562 cell line incubated for 4 hours and B, D were images of treated K562 cell line incubated for 6 hours.

Figure 5.33 Confocal fluorescence micrographs of DSB (A, B) and optimized DSB-PLGA-Ch-GNPs nanoformulation (C, D) in K562 cell line

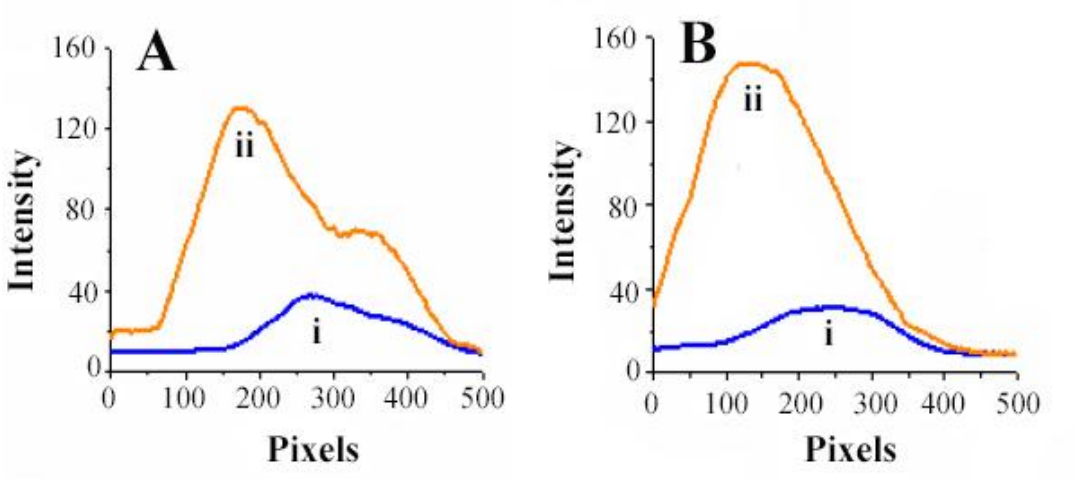

(i - DSB and ii - optimized DSB-PLGA-Ch-GNPs nanoformulation)

Figure 5.34 Quantitative fluorescence intensity curves of DSB and optimized DSB-PLGA-Ch-GNPs nanoformulation for 4 hours (A) and 6 hours (B)

5.4.10 *In vitro* cytotoxicity assay

To investigate the cell viability *in vitro* cytotoxicity study was performed for the optimized nanoformulation (DSB-PLGA-Ch-GNPs), reference standard and pure drug by sulforhodamine B assay. It was performed against K562 human myeloid leukaemia cell lines to compare the percentage cell growth and percentage growth inhibition by optimized nanoformulation as compared to control, standard drug (adriamycin) and the pure drug (DSB). The percentage control growth vs. drug concentration profiles are shown in Figure 5.35. The optimized formulation exhibited significantly more % growth inhibition as compared to DSB. This indicates that the optimized nanoformulation exhibits a potential cytotoxic effect in the treatment of CML.

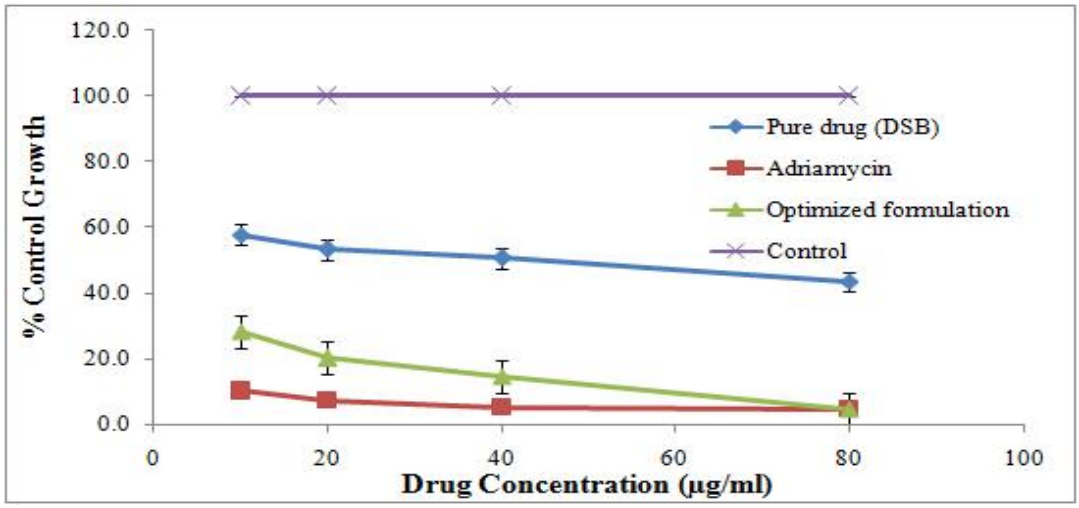

(vertical bars represents mean ± SD, n = 3, $p<0.001$ compared to pure drug, Two-way ANOVA, Bonferroni post-test)

Figure 5.35 Percentage control growth versus drug concentration (µg/mL) profiles

5.4.11 Cell apoptosis assay

Apoptosis or the programmed cell death is the process of removal of unwanted cells thereby conserving the key proteins. Apoptosis occurs due to a cascade of events, and apoptotic cells can be identified by morphological features like cell shrinkage, chromatin condensation, nuclear envelope disintegration and formation of irregular bulges in the cell membrane. Flow cytometry is used to quantify the number of

apoptotic cells in a clinical sample by making measurements on each individual cell. It is based on a study of a total cell population that averages the results from every given cell. The effect of optimized nanoformulation (DSB-PLGA-Ch-GNPs) on the induction of apoptosis were evaluated with PI and annexin V–FITC by increasing concentration of the optimized nanoformulation (0, 5, 10 and 15 µg/ml) and exposure time (6, 12 and 24 hours). The flow cytometry results revealed that with the increase in the GNPs concentration and exposure time, the apoptosis was also increased in the cell population, suggesting that the GNPs could exert effective antileukaemia activity against K562 cells and further induce the K562 cell death with a dose and time dependent manner (Figure 5.36 and Figure 5.37).

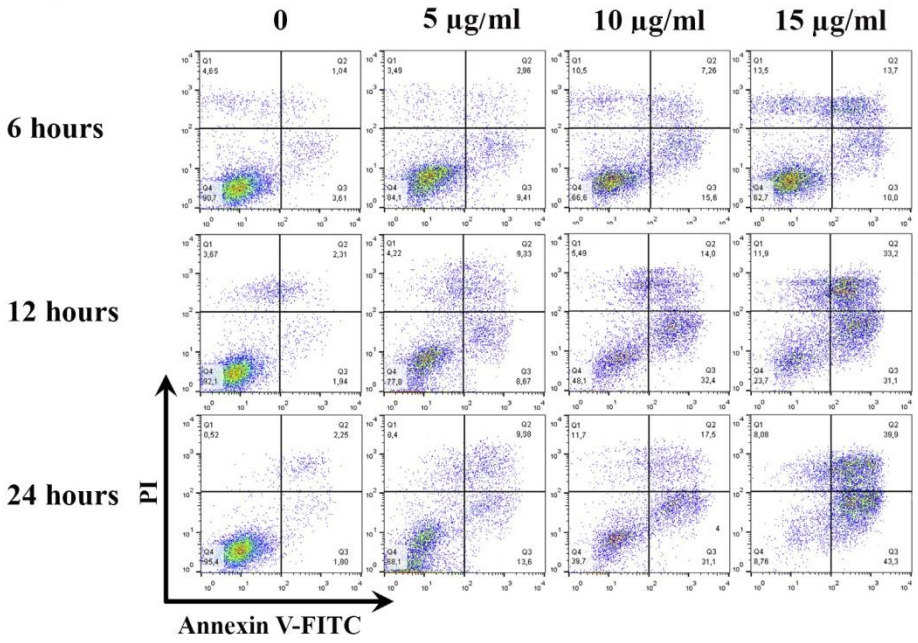

Figure 5.36 Dot plot of apoptosis in K562 cell line detected by flow cytometry

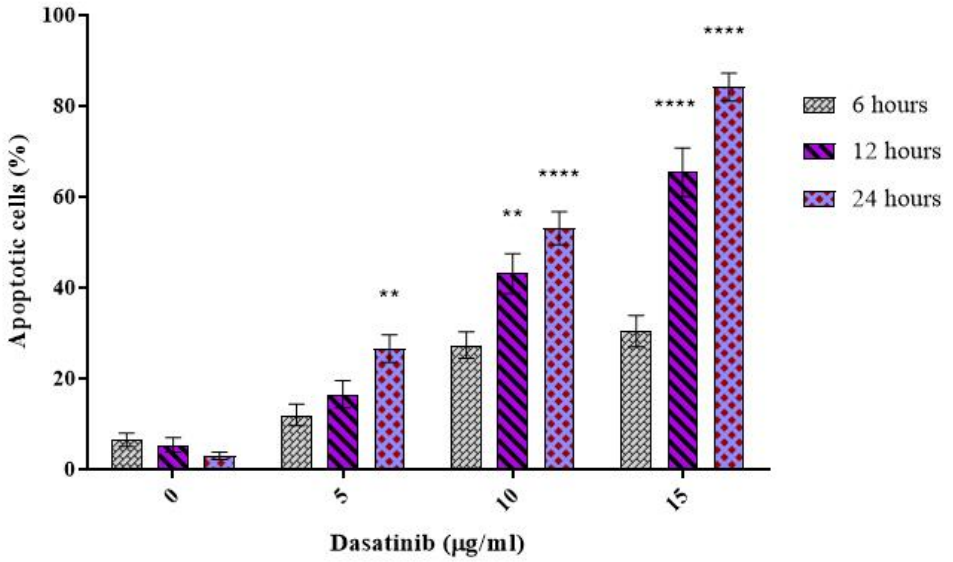

(vertical bars represents mean ± SD, n = 4; ** p<0.01, ****p<0.0001, Bonferroni post-test)

Figure 5.37 Bar graph displaying the percentage of apoptotic cells at different concentrations of optimized DSB-PLGA-Ch-GNPs nanoformulation and exposure times

5.4.12 *In vivo* pharmacokinetic study

Pharmacokinetic study was carried out to measure the bioavailability and estimate the pharmacokinetic parameters. Plasma drug concentration vs. time profiles of pure DSB and optimized nanoformulation (DSB-PLGA-Ch-GNPs) is shown in Figure 5.38 and it's pharmacokinetic (PK) parameters in Table 5.21. The results of *in vivo* pharmacokinetic study distinctly revealed that there was a significant difference in the pharmacokinetics of DSB when administered in the form of GNPs. The non-compartmental analysis of pure DSB and the optimized nanoformulation was carried out using Kinetica 5.1 software. The Cmax of optimized nanoformulation was found to be 1.33 times lower than that of pure DSB suggesting the reduced intensity of adverse effects related to high dose. Optimized nanoformulation showed much larger AUC (7.4 fold), MRT (11.26 fold), and $t_{1/2}$ (13.41 fold) than the pure DSB which itself is indicative of more bioavailability of DSB-GNPs and also have longer retention in the

circulatory system and therefore found to be more effective drug delivery system in the treatment of CML.

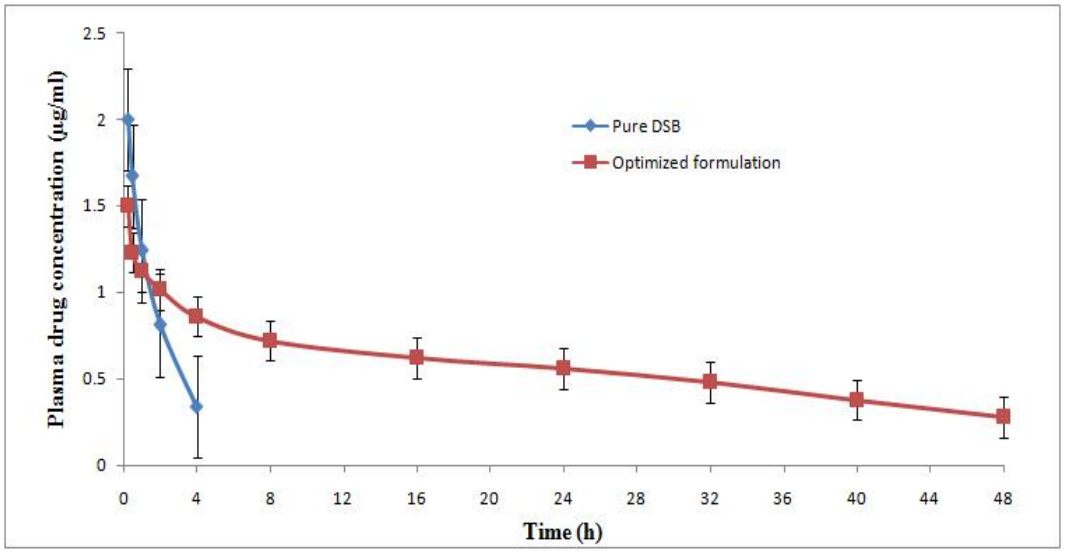

(Vertical bars represents mean ± SEM, n = 6)

Figure 5.38 Plasma drug concentration Vs. time profile of pure DSB and optimized DSB-PLGA-Ch-GNPs nanoformulation in rats

Table 5.21 Pharmacokinetic parameters calculated for pure DSB Vs optimized DSB-PLGA-Ch-GNPs nanoformulation

Parameter	Pure DSB	Optimized nanoformulation
C_{max} (µg/ml)	2 ± 0.63	1.5 ± 0.24
T_{max} (h)	0.25 ± 0.12	0.25 ± 0.08
$AUC_{(0-t)}$ (µg-h/ml)	4.599 ± 0.92	34.181 ± 1.26
MRT (h)	1.605 ± 0.54	18.080 ± 0.98
$t_{1/2}$ (h)	2.24 ± 0.86	30.06 ± 1.14

C_{max} - maximum plasma concentration; T_{max} - maximum time to achieve peak plasma concentration; $t_{1/2}$ - elimination half life; MRT - mean residence time and $AUC_{(0-t)}$ - area under the curve from zero time to last sampling time t.